9950-1357

FAIRCHILD
SPACE

FSC-ESD-217-88-435

IN-31-CR
52251
p-69

CENTAUR IN-TANK EXPLOSION FLOW FIELDS WITHIN STS AND TITAN IV PAYLOAD SPACES

M. ECK
M. MUKUNDA

DECEMBER, 1988

(NASA-CR-189039) CENTAUR IN-TANK EXPLOSION FLOW FIELDS WITHIN STS AND TITAN 4 PAYLOAD SPACES Interim Report (Fairchild Space Co.) 69 p
CSCL 13B
N92-12144
Unclas
G3/31 0052251

FAIRCHILD SPACE • 20301 CENTURY BOULEVARD • GERMANTOWN, MARYLAND 20874

FSC–ESD–217–88–435

CENTAUR IN-TANK EXPLOSION FLOW FIELDS WITHIN STS AND TITAN IV PAYLOAD SPACES

INTERIM REPORT, JPL CONTRACT 957524

M. ECK
M. MUKUNDA

This report was prepared for the Jet Propulsion Laboratory, California Institute of Technology, sponsored by the National Aeronautics and Space Administration.

DECEMBER, 1988

TABLE OF CONTENTS

LIST OF FIGURES

Page

Page

Page

LIST OF TABLES

I. INTRODUCTION AND SUMMARY

The effort described in this report was commissioned by the Jet Propulsion Laboratory (JPL) in 1986 under JPL Contract 957524. The initial thrust of this effort involved attempts to reconcile the experimental results reported in the Project PYRO documentation [1] with theory. The initially contracted effort was expanded after the STS-51L (Challenger) event to cover a number of Galileo Radioisotope Thermoelectric Generator (RTG) safety issues. This additional material is reported in FSC-ESD-217-88-426 and FSC-ESD-217-89-457. The material in this report deals with explosions resulting from the mixing of liquid hydrogen and liquid oxygen (LH_2-LO_2) such that the reactants are confined by the missile (CBM) body. Explosions which were confined by the ground surface (CBGS) were also studied and the results of these studies are presented in the companion reports referenced above.

Initial attempts to predict the reported PYRO experimental results were unsuccessful. A new reaction-energy-addition hypothesis was then developed and tested. The results obtained using this hypothesis provide reasonable agreement with the experiments both in the near and far field. This hypothesis also allows reconciliation of the apparent discrepancy observed by others [2, 3] in the near field static overpressure and impulse.

Calculations were performed to predict the environment which would occur at the Galileo RTG location given a Centaur G' upper stage and an STS launch vehicle. It was concluded that the principal threat to the RTG in this environment would be the impact of a slug of liquid hydrogen. No analyses were conducted to assess the response of the Galileo RTG to such an environment. This study was stopped when a programmatic decision was made to replace the Centaur G' with the IUS as the Galileo injection stage.

Some concern was expressed that the expansion of the liquid cryogens from a Centaur G' failure (absent an explosion) could threaten the integrity of the Galileo plutonia containment system. Detailed calculations were performed using the Centaur G' in the STS-Bay geometry. These calculations showed that the flow field resulting from the failure of the Centaur G' tankage was quite benign. It was concluded that while the cryogen particle velocity was very high the flow field density was extremely low. As a result the dynamic pressure was a trivial eight psia.

The Centaur G' CBM case was revisited when alternative plans were addressed for launching Galileo on a Titan IV booster. This study showed results similar to those predicted for the Centaur G' STS-Bay case. Peak static overpressures of less than 900 psi were predicted at the RTG location; however, the liquid hydrogen slug problem reappeared. These later calculations were refined to provide information for the Titan IV RTG launch environment data book [4]. A Monte Carlo analysis was performed using JPL personnel supplied probability density distributions for potential reactant mass and reactant charge density. The maximum local static overpressure drawn in the Monte Carlo was 640 psi. This value is well below the 2000 psi environment created in the shock tube tests which were conducted on the GPHS plutonia containment system. The response of a GPHS RTG to the impact of a slug of liquid hydrogen was not predicted although the environment was defined in sufficient detail to allow analytical and experimental verification.

II. TECHNICAL DISCUSSION

The material in this chapter is organized in the chronology in which it was performed. The Project-PYRO analyses were conducted first to provide a sound basis for the subsequent effort. The PYRO analyses showed that there is most likely a considerable amount of gaseous hydrogen deflagration in air following an initial prompt energy addition (explosion). This deflagration is not treated in the subsequent Centaur G' CBM calculations although after-burning of the prompt reaction products is. Additional PRYO analyses should be performed to evaluate this effect and the reaction mass required to produce these environments should be determined especially if the observed explosion involves only gaseous reactants.

The material in this chapter is divided into four sections:

A. Project PRYO Analytical Simulation
B. Environments Created by Centaur G' Explosion in the STS-Orbiter Bay
C. Environments Created by the Expansion of Liquid Cryogens into Vacuum Absent Explosion
D. Environments Generated by a Centaur G' Explosion under a Titan IV Payload Fairing

Detailed discussions of the above topics are presented in the following sections.

A. Project PYRO Analytical Simulation

Project PYRO [1] was an extensive experimental program conducted in the early and mid 1960s to establish siting criteria for facilities constructed in support of the Apollo program. A number of anomalies in the results presented by the authors have been reported by other investigators [3,5,6]. Initial attempts made by the authors to duplicate the referenced PYRO-CBM experimental results also were unsuccessful. As more became known about how the PYRO-CBM experiments were conducted, it became apparent that the analysts and the experimentalist were making assumptions about the manner in which the experimental results were obtained which were not faithful representations of the physical realities of the experiments. Once analytical models were formulated which were accurate representatives of the physics of the PYRO events, good agreement between the predicted and observed results were obtained.

A discussion of the inconsistencies observed in the reported PYRO results as well as analytical-model-guided interpretations of what probably occurred in the PYRO-CBM events are presented in the following sections.

1. Problem Statement

The PYRO-CBM results were reported as "static" pressure and impulse as a function of range from the center of burst. The reported results did not account for the fact that the Kistler gages used to make the pressure measurements were located in the ground plane. Further, no measurements (direct or indirect) were made of dynamic pressure. Time of arrival measurements, were made, but were not reported because of apparent inconsistencies in the results. As a result, it is impossible to perform even the most rudimentary sanity checks on the reported results.

Other investigators [3,6] attempted to reconcile the near- and far-field static pressure and impulse reported by the PYRO-CBM experimenters. They concluded (correctly) that it was impossible to reconcile the reported near and far-field environments if one assumed a single mechanism (detonation) for the event's energy addition mechanism.

The deficiencies observed in the PYRO-CBM test protocols were serious in that they directly determined the RTG explosion-environments. It was concluded that a detailed review of the PYRO test procedures, data acquisition methods, reporting methods, and data reduction methods should be undertaken. A complete, but as yet unpublished evaluation of project PYRO conducted by WSTF personnel [7] is the definitive work in this area. These investigators concluded, as had the authors independently, that neglecting height of burst and dynamic pressure effects on the "static" pressure gages introduced serious errors into the reported results.

The work presented in the following paragraphs attempts to correct the project PYRO results for ground plane, height of burst and burst symmetry problems which were not properly addressed in the original reports. In addition a hypothesis is presented which reconciles the apparent anomalies in the reported near-field and far-field results.

2. Analytical Simulation of Confined by Missile Events (CBM)

A detailed axisymmetric PYRO-CBM event model was prepared. The general arrangement of the materials simulated in this model is shown in Figure 1. Tankage shells were not included in the model. A volume burn of the reactants was assumed. The effects of various energy additions were investigated as was the effect of height of burst.

Initial attempts to match the PYRO-CBM calculated and observed LH_2-LO_2 explosion environments were unsuccessful. Sensitivity studies were performed to determine the effect on the reported side-on (static) pressure of reaction energy, reaction density height-of-burst and the location of the test pressure transducers. The results of these sensitivity analyses are presented in Table I.

a. Height of Burst Effects. The basic problem noted in the tabulated results is the effect of height-of-burst on the reported side-on-pressure. It is impossible to reconcile the one-charge diameter results with those observed in the far-field if one assumes that the reported pressures are actually side-on pressures. The best fit of the analytical predictions to the experimental data occurred, for one-charge diameter (1-D), when a 2.5 percent-of-reactants charge mass having a density of 0.1 gm/cc was volume burned in the LO_2 ullage with an average energy addition of 1050 cal/gm.

Examination of Figure 2 shows that while a calculation using this set of assumptions matches pressures rather well, it grossly underpredicts impulse. Clearly, there must be a

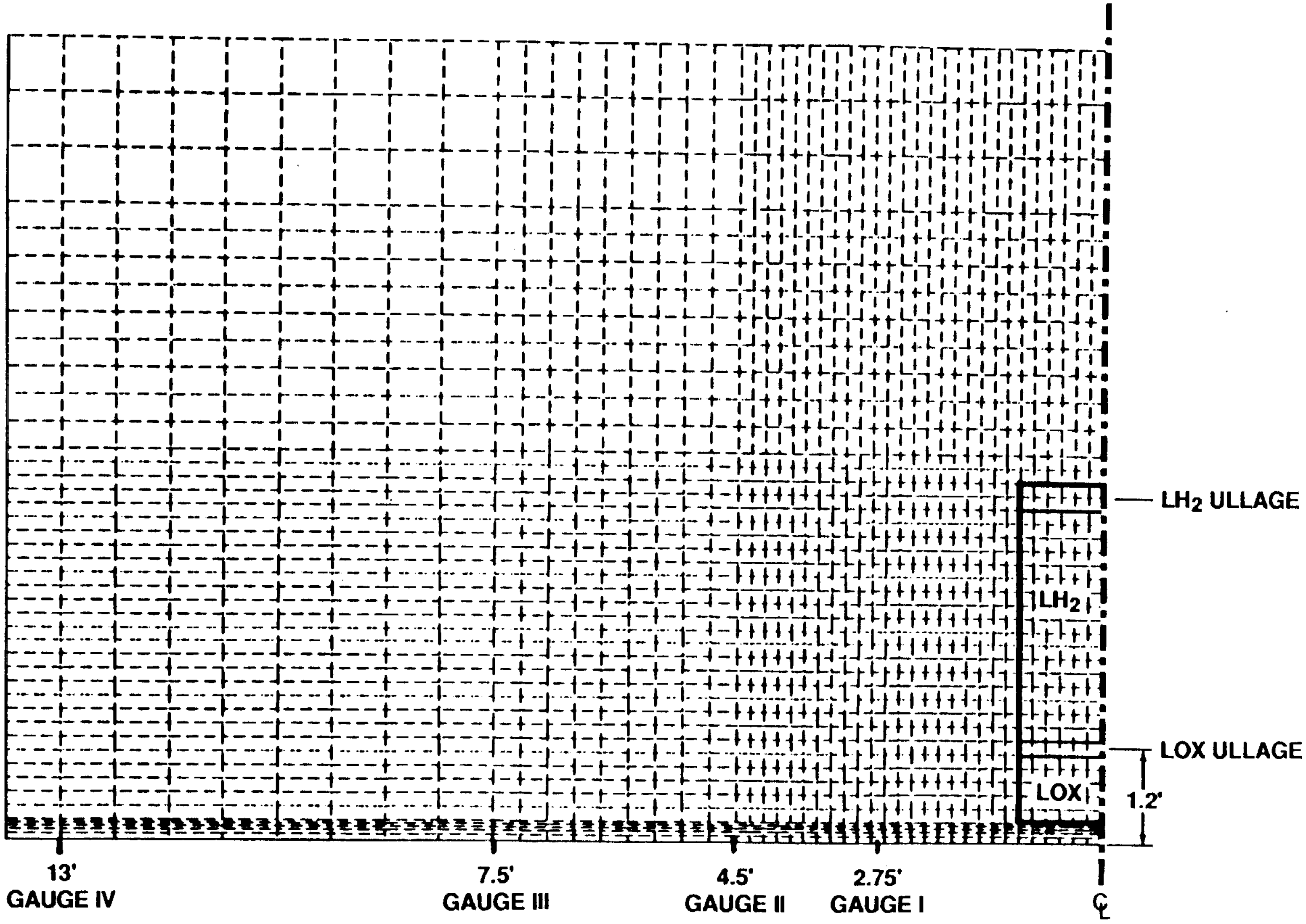

Figure 1. Pyro CBM Axisymmetric Euler Grid and Tank Model

Table I. Summary of Pyro Test Simulation(1)

DATA SET	REACTION MASS	SIE	REACTION(2) ENERGY	REACTION DENSITY	HEIGHT OF BURST ℄ ABOVE GROUND PLANE	PEAK OVER PRESSURE @ 2.75 FT.	RATIO WALL/ NO WALL	PEAK OVER PRESSURE @ 4.5 FT.	RATIO WALL/ NO WALL
	LBS.	CAL/GM	10^6 CAL	GM/CC	FT	BARS		BARS	
355 TEST	5	355	.80	0.1	1.2	9.0	3.0	3.6	1.84
355 NO WALL(3)	5	355	.80	0.1	1.2	3.0		1.95	
1050 TEST	5	1050	2.37	0.1	1.2	38.0	3.7	10.4	1.92
1050 NO WALL	5	1050	2.37	0.1	1.2	10.2		5.4	
2100RHP1	5	2100	4.75	0.1	1.2	70	3.9	—	—
P12100 NO WALL	5	2100	4.75	0.1	1.2	18		—	
1050RHP2	10	1050	4.75	0.2	1.2	54	3.6	14	1.75
P2 1050 NO WALL	10	1050	4.75	0.2	1.2	15		8	
LOW 1050	5	1050	2.37	0.1	0.8	33	2.75	—	—
LOW 1050 NO WALL	5	1050	2.37	0.1	0.8	12		—	

[1] PYRO MODELED AS AXI-SYMMETRIC TANK WITH FLAT ENDS. REACTION INITIATED IN ULLAGE VOLUME. ~180 LBS. LOX, 36 LBS. LH_2 MODELED.

[2] ENERGY ADDED TO ALL REACTANTS OVER A 400 μSEC PERIOD. PRESSURE CALCULATED BY: $P = (\gamma - 1)(\rho)$ SIE

[3] NO-WALL CASES ARE IDENTICAL TO THEIR PAIR EXCEPT A FLOW BOUNDARY IS INTRODUCED AT THE MODEL GROUND PLANE.

S-199 09L 8 90C

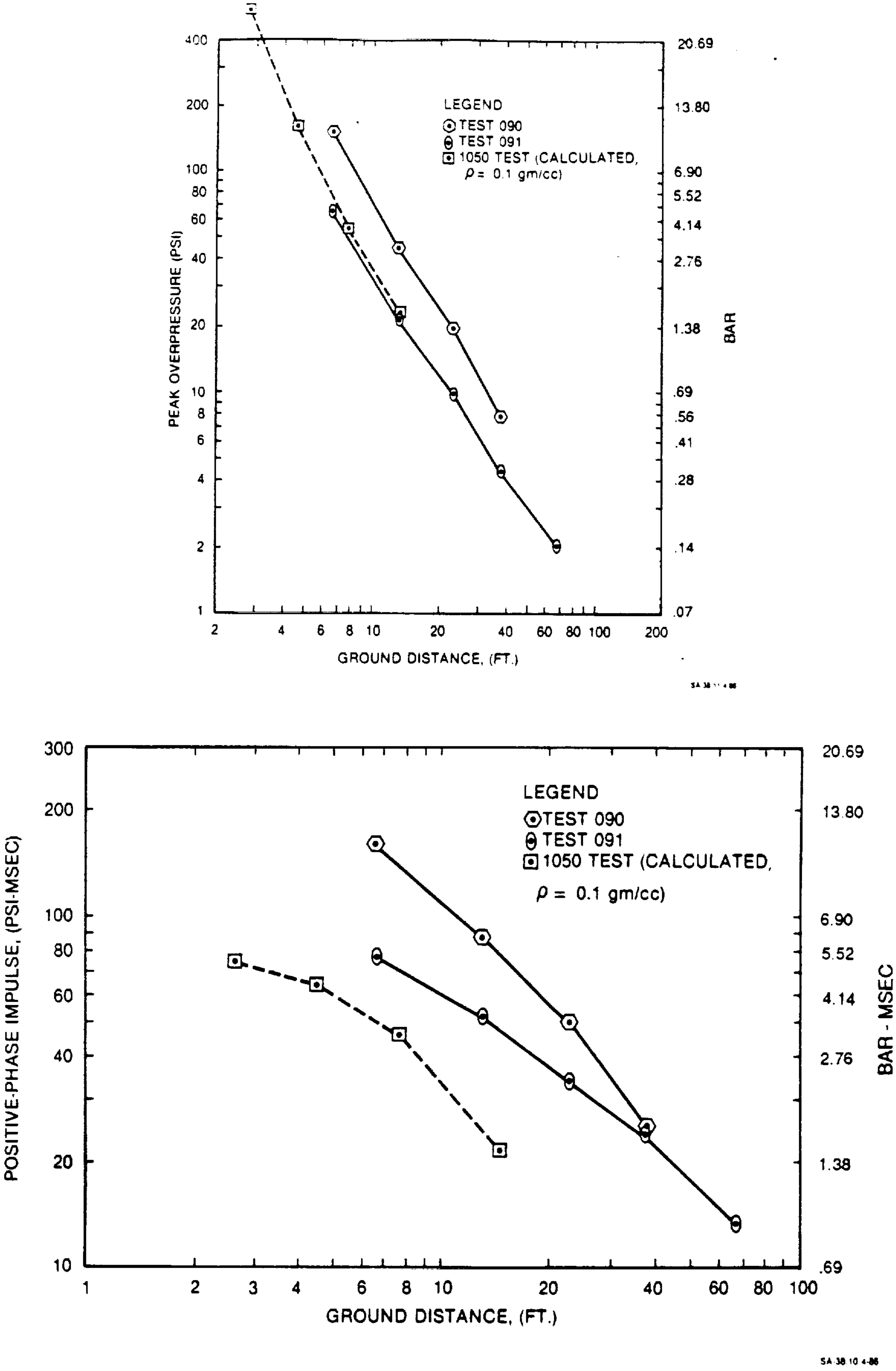

Figure 2. Comparison of Calculated Side-On (Static) Overpressure and Impulse to Experimental Observation.

mechanism at work which prevents the normal triangular shaped pressure drop off behind the shock from occurring. Initial efforts to identify this mechanism centered on the manner in which the side-on pressure instrumentation was configured.

The location of the Kistler gages in the ground plane caused a significant reflected pressure component to be included in the reported side-on pressures. Calculations were conducted to assess the magnitude of the reflected pressure effect. These calculations used the simple devise of providing either a flow boundary or a reflecting (wall) boundary along the model ground plane. The effect of height-of-burst could then be isolated by holding all other model variables constant while adding or subtracting the ground plane. The effect of the ground plane boundary assumption on the resultant explosive flow field is readily apparent at the time of peak gage-pressure in Figure 3. Similar results were obtained for parametric variations in the explosive-reaction conditions. The results of these parametric calculations are presented in Table I. Peak side-on pressure drop off as a function of distance from the charge center for the cases calculated is shown for the flow and no-flow boundary cases in Figure 4. Figure 4 also shows the peak side-on pressure ratio for the ground plane (wall) and no ground plane (no wall) cases. It is clear from the results of these calculations that inadvertent measurement of reflected pressure caused the reported PYRO-CBM side-on pressure to be overstated by a factor of 3.0 to 3.8 at the 2.75 foot gage location. Further examination of the results of these calculations shows that the ground plane (wall) effect was negligible, 13 feet from the tank centerline.

b. Impulse Reconciliation. While the above calculations went a long way in reconciling the reported PYRO-CBM results with theory, they still did not account for the observed discrepancies in reported impulse. Because of the method used to initiate reactant mixing in the PYRO-CBM test set-up, there is a high probability that the explosion occurred in or near the LO_2 ullage space

Initial reactant mixing will cause large quantities of hydrogen gas to be generated. The dynamic pressure created by this gas generation followed by an explosion at the LO_2 ullage site has the effect of accelerating large quantities of reactants in opposite directions. This

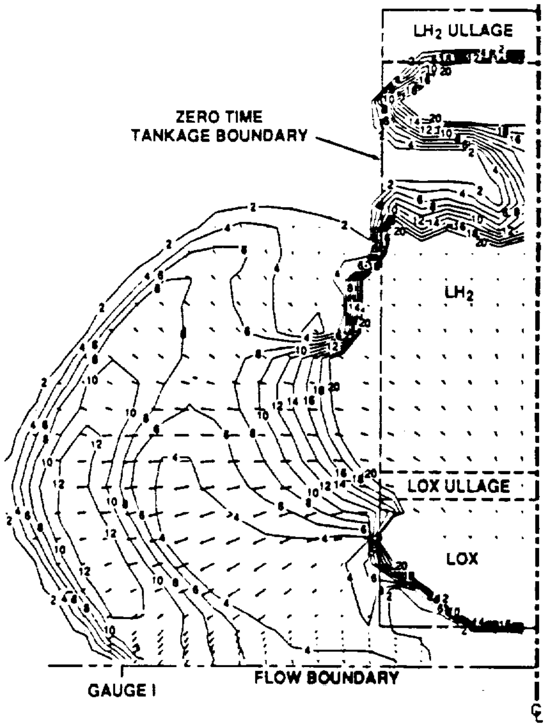

Pressure, Bars - No Ground Effect
(1050 cal/gm; ρ = 0.1 gm/cc; 1050NoWall)

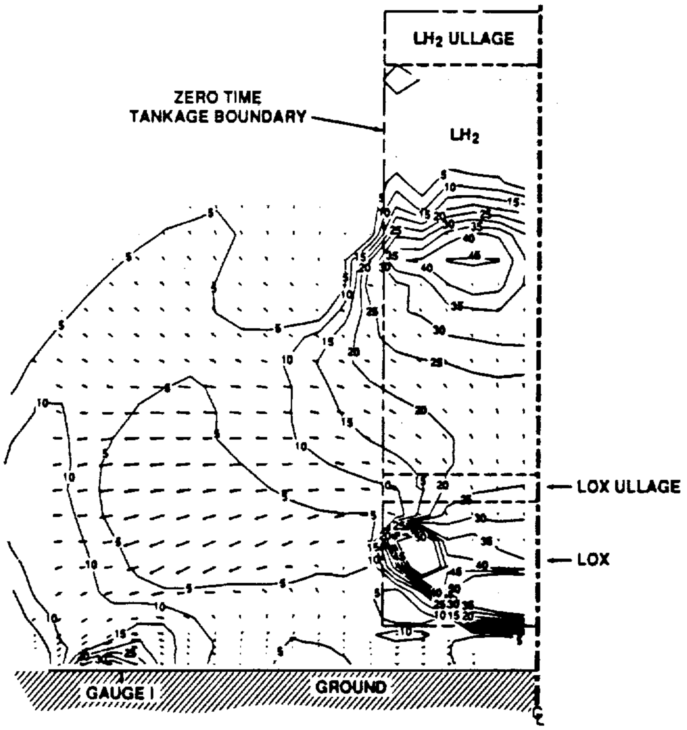

Pressure, Bars - With Ground Effect
(1050 cal/gm; ρ = 0.1 gm/cc; 1050Test)

S-199.05C 7/90M

Figure 3. Axisymmetrical Flow Field at Time of Peak Static Pressure
5 Lb. of LH_2 - Lox Reactants

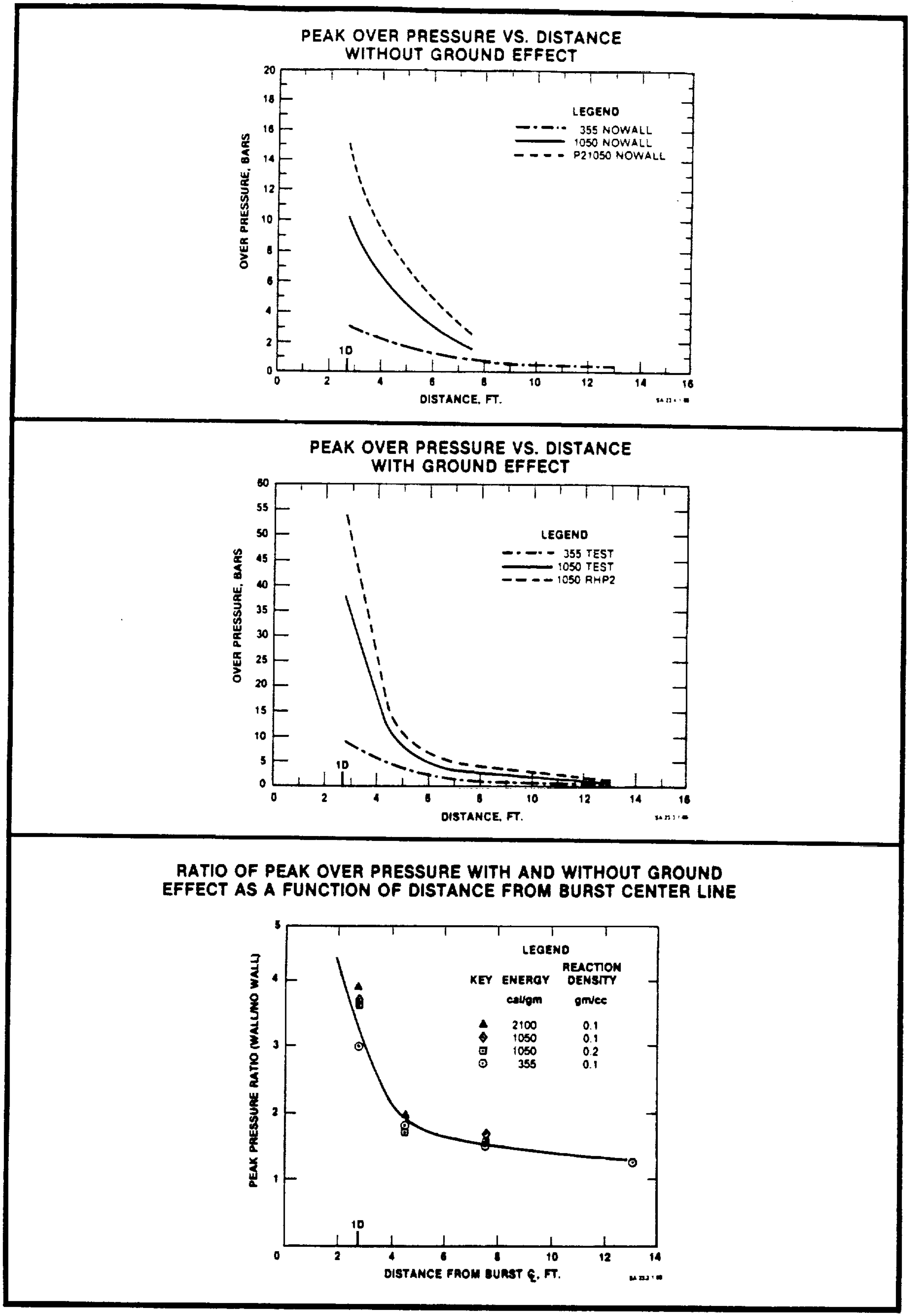
PEAK OVER PRESSURE VS. DISTANCE WITHOUT GROUND EFFECT

PEAK OVER PRESSURE VS. DISTANCE WITH GROUND EFFECT

RATIO OF PEAK OVER PRESSURE WITH AND WITHOUT GROUND EFFECT AS A FUNCTION OF DISTANCE FROM BURST CENTER LINE

S-199.06C 12/89M

Figure 4. Analytical Assessment of the Effect of Height-of-Burst on the reported Pyro-CBM Experimental Observations.

scenario results in a totally different flow field than would result from the detonation of a condensed explosive. This different phenomenolgy causes the reaction energy release to occur in two-distinct phases:

1) A prompt yield from the ignition of the LH_2-LO_2-GH_2-GO_2 froth created by reactant mixing.

2) A delayed yield from the vaporization and burning in air of the residual LH_2.

Such a scenario would cause the peak static overpressure in the near field to be controlled by the prompt yield while the far-field static overpressure would be determined by the event's total energy addition. Residual LH_2 vaporization and deflagration in air will have the effect of increasing the event's total energy addition and prolonging the positive phase impulse without raising the near-field peak static overpressure.

For these reasons, a more promising analytical approach would be to abandon the single-mechanism energy-addition model and treat the event as two concurrent phenomena occurring in grossly different time domains. A graphical representation of the proposed approach is presented in Figure 5 along with a schematic pressure-time history showing the effect of hydrogen after-burning on positive phase impulse. Unfortunately, neither the pressure-time traces nor time-of-arrival information were available for the PYRO-CBM tests of interest. As a result, it was not possible to approximate the relationship between implied particle velocity and observed impulse.

A model which used the Figure 5 energy addition scheme only for the initial reaction products was devised and executed. The results obtained using this model are discussed in subsequent paragraphs.

c. Phased Energy Addition Models. The first energy addition model simply burned the hydrogen involved in the explosive reaction in the LO_2 ullage to completion. A histogram of the energy addition is shown in Figure 6. The energy addition to the initial reactants was

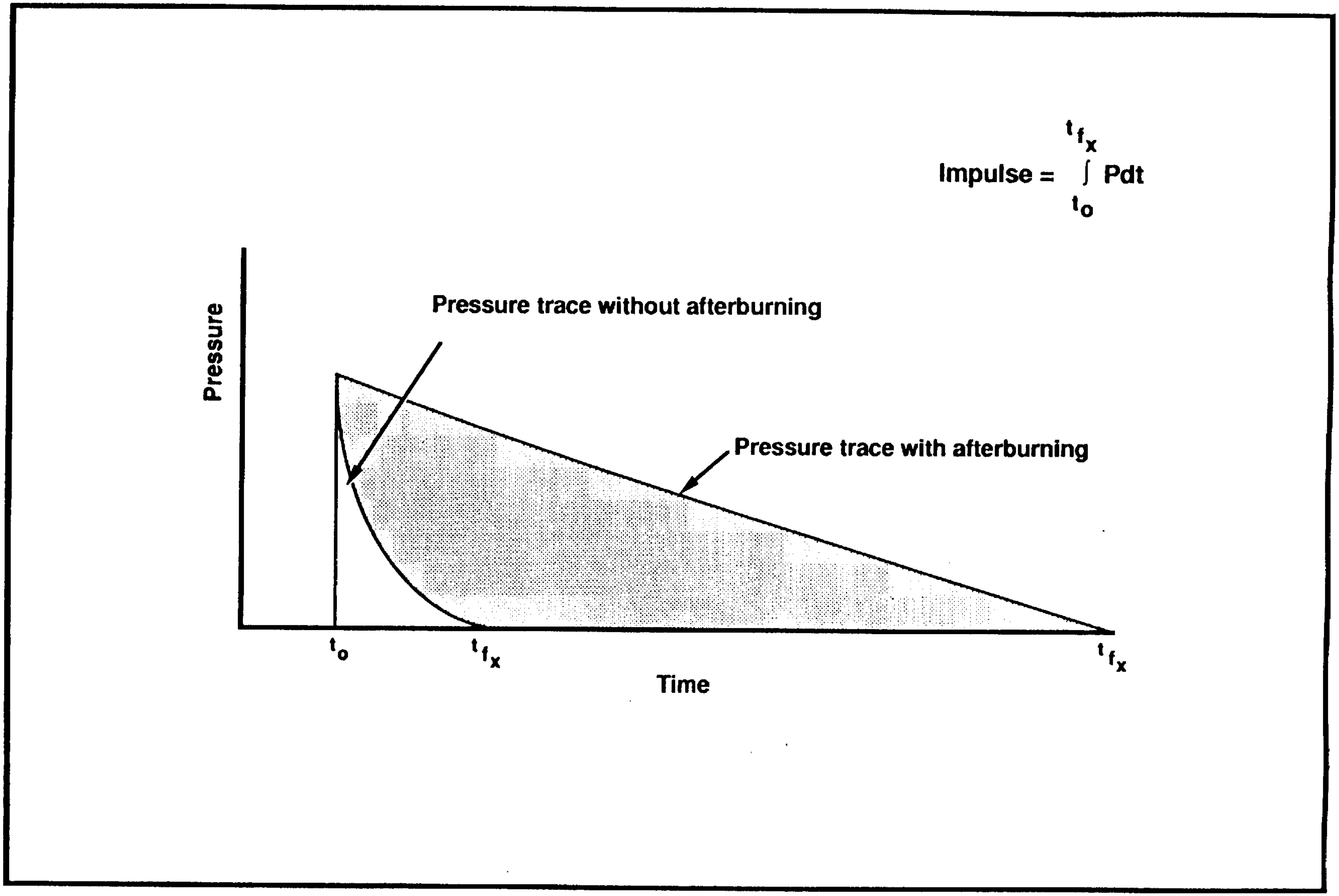

S-199.07C 3/90M

Figure 5. Schematic Representation of the Effects of Staged Energy Addition.

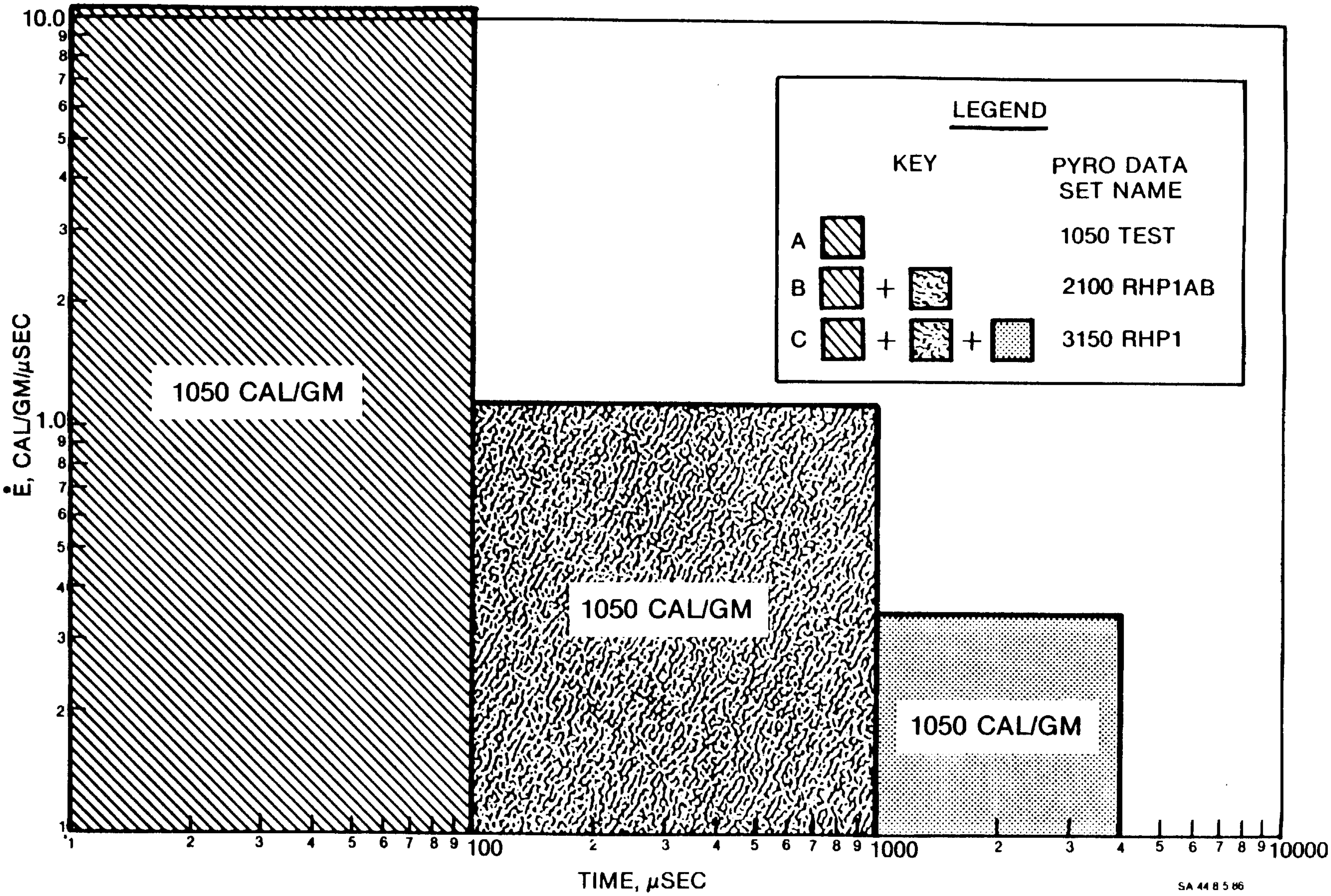

Figure 6. Initial Staged-Model Energy Addition ($\dot{E}$) Profile (5 lb. of Pyro Reactants; $\rho = 0.1$ gm/cc)

carried out in three steps: 1) from zero to 100 μsec (prompt phase); 2) from 100 to 1000 μsec; 3) from 1000 to 4000 μsec (delayed phase). The charge density used in these calculations was 0.1 gm/cc and the charge mass was 2.5 percent of the available reactants. The late time flow field and material locations resulting from exercising this model are presented in Figure 7.

Subsequent evaluations showed that the predicted impulses still did not match the PYRO-CBM observations. A more complex energy addition profile was then devised. It was reasoned that in a LO_2 ullage explosion, the residual LH_2 which was accelerated away from the LO_2 would still vaporize and burn in air. Two models were prepared and executed to evaluate this premise. Both of these models separated the residual hydrogen into two zones: the "surface" hydrogen; and the "core" hydrogen. It was reasoned that the surface hydrogen would see the surrounding air earlier in time than would the core hydrogen. The time at which energy addition began in the surface and core hydrogen as well as the percent completion of their deflagration in air was arbitrarily assumed. The manner in which the energy addition was accomplished is shown graphically in Figure 8. The time zero locations of the various reactants are shown in Figure 9. The calculations were then performed and the results are presented in Table II. The pressure-distance and impulse-distance traces from the analytical models were compared to experimental observations. The results of these comparisons are presented graphically in Figure 10.

One final calculation was performed to assess the adequacy of the Euler zoning. Calculations of the type undertaken are subject to substantial numerical diffusion. The net effect of too large zoning is to decrease the value of the predicted peak pressure while conserving momentum (impulse). Examination of Figure 10 shows that some zoning problems are occurring. The "micro zone" case and the 1050-10lb - 700 case have identical energy addition profiles. If the change in zoning is not important the reported pressure-distance traces would be identical. Since they are clearly not identical, one may assume that the zoning used for all cases other than "microzone" was too course. As would be expected, there is little effect of zoning on the impulse curves shown in the second panel of Figure 10.

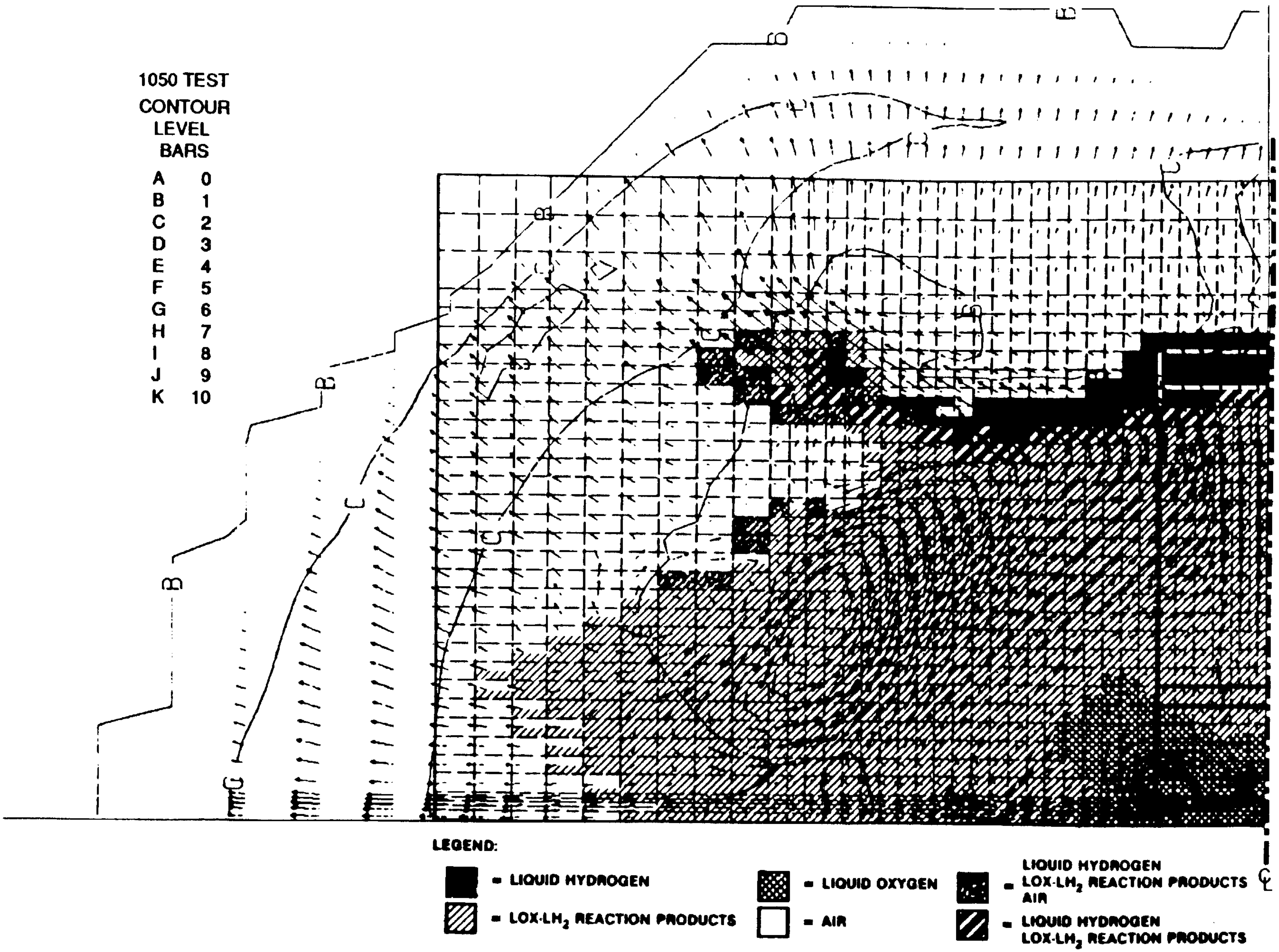

Figure 7. Predicted Pyro Flow Field Using Initial Energy Addition Model

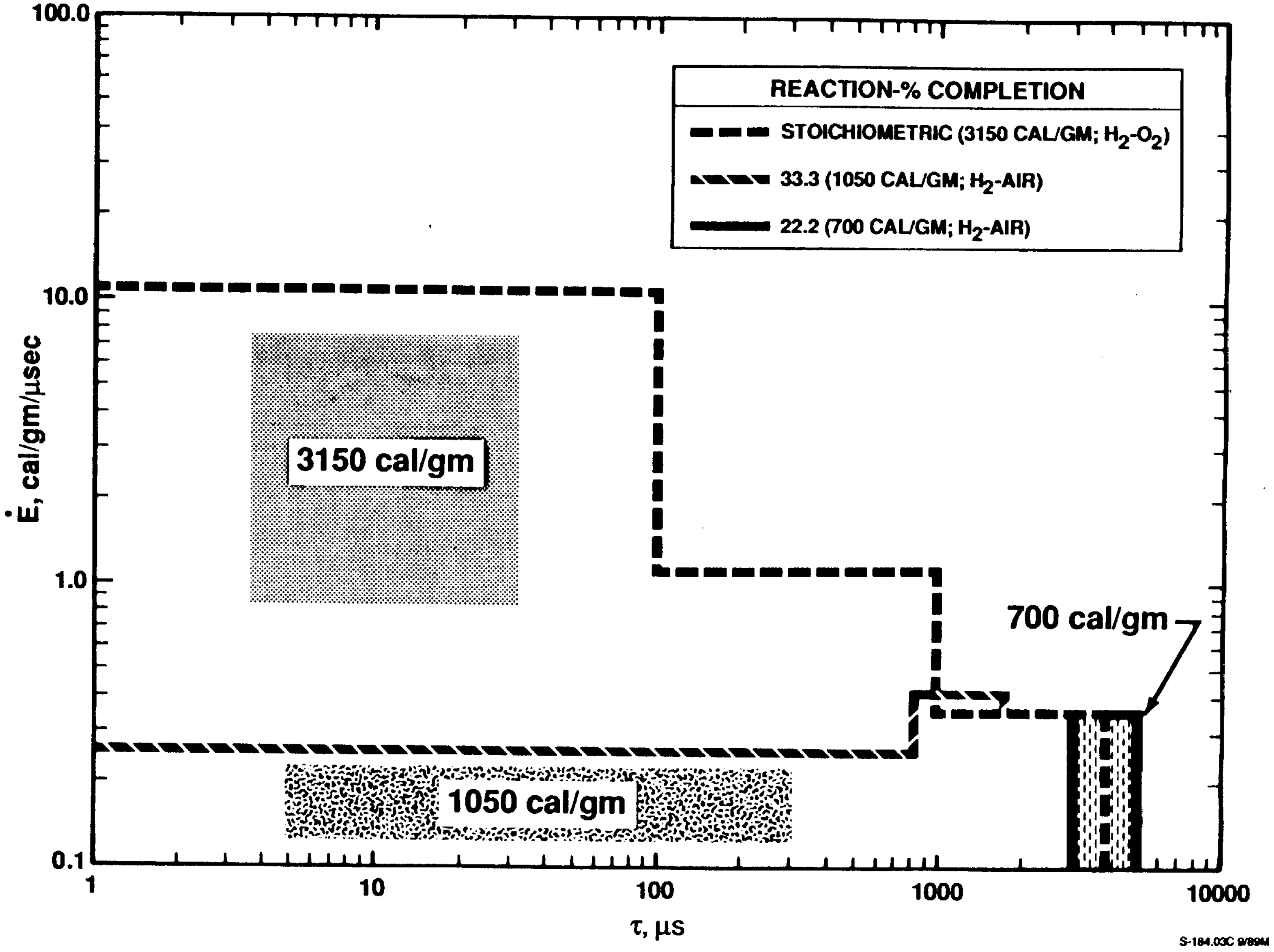

Figure 8. Final Staged-Model Energy Addition ($\dot{E}$) Profile (5 lb. of Pyro Reactants; ρ = 0.1 gm/cc)

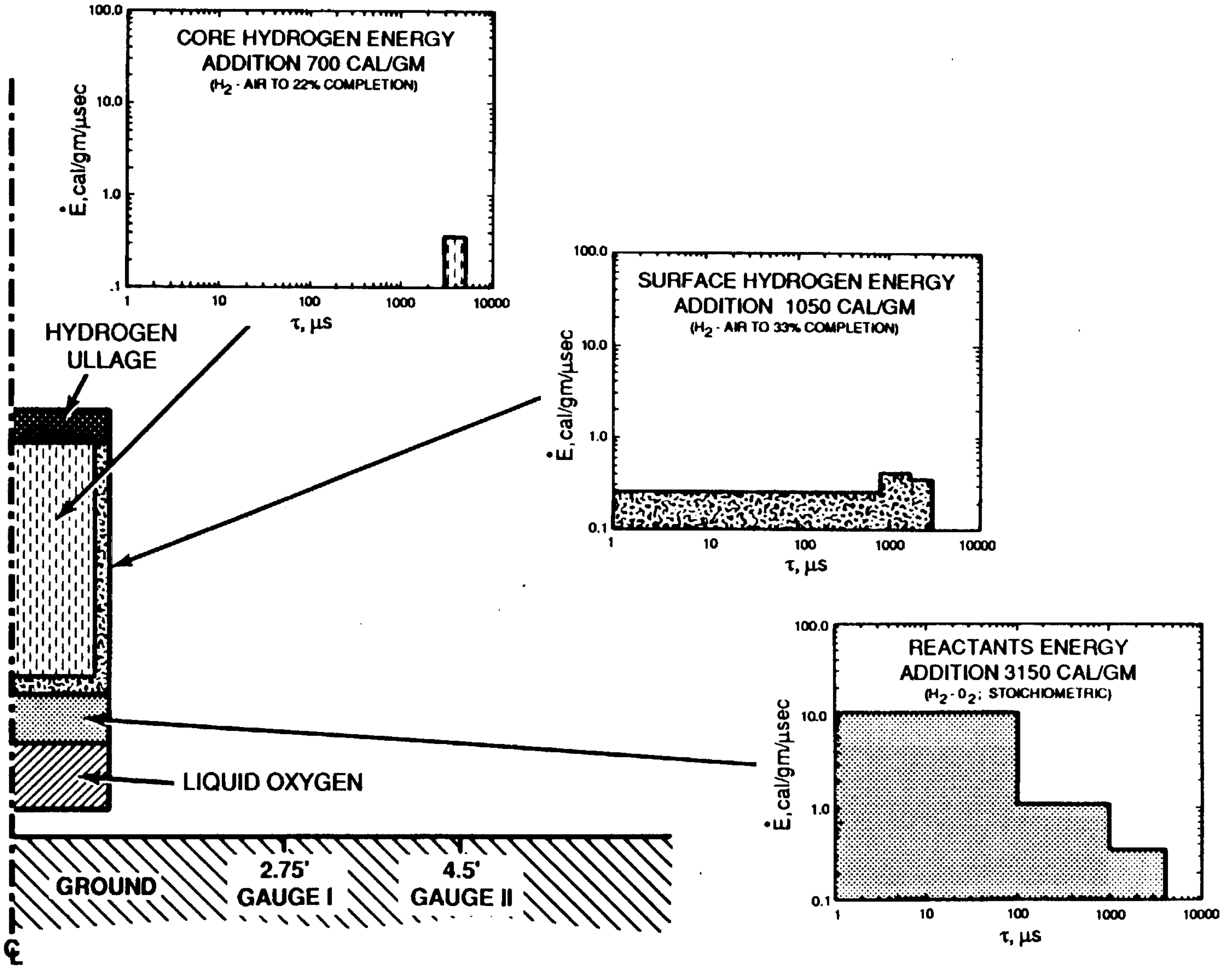

S-184.04C 9/89M

Figure 9. Pyro Test 90 and 91 Flow Field Simulation (10 lb. Reactants; 35lb. LH_2 ; 150 lb. LOX; Time Zero)

Table II. Summary of Effect of Prompt Energy Addition Rate on Pyro Simulation Results(1)

DATA SET	REACTION MASS	REACTION ENERGY	ENERGY ADDITION PROFILE(2)	PEAK OVER-PRESSURE @2.75 FT	STATIC IMPULSE @2.75 FT	PEAK OVER-PRESSURE @4.5FT	STATIC IMPULSE @4.5 FT
	LBS	10^6CAL		BARS (PSI)	PSI-MSEC	BARS (PSI)	PSI-MSEC
1050 TEST	5	2.37	A	38 (551)	75	10.4 (151)	62
2100 RHP1	5	4.75	A	92 (1334)	125	-	-
2100 RHP1AB	5	4.75	B	53 (768)	116	16.5 (239)	84
3150 RHP1	5	7.12	C	53 (768)	159	16.5 (239)	116
987__5LB350	5	7.12	C	45 (659)	225	16.5 (239)	203
1050__10LB700	10	14.24	C(3)	65 (950)	280	19.3 (280)	250
BIGEUL	10	14.24	C(4)	90 (1305)	312	26.5 (384)	260

S-199.02C 2-90C

1) PYRO MODELED AS AXI-SYMMETRIC TANK WITH FLAT ENDS. REACTION INITIATED IN ULLAGE

2) ENERGY ADDED PER SCHEDULE SHOWN IN FIGURE 9.
REACTION DENSITY = 0.1 gm/cc; HEIGHT OF BURST = 1.2 FT; AVAILABLE CRYOGENS MODELED ~180 LOX,36 LB LH_2.

3) EXCESS HYDROGEN BURNED IN AIR. NET ENERGY ADDITION = 16.8 × 10^6 CAL.

4) EXCESS HYDROGEN BURNED IN AIR. NET ENERGY ADDITION = 27.4 × 10^6 CAL.

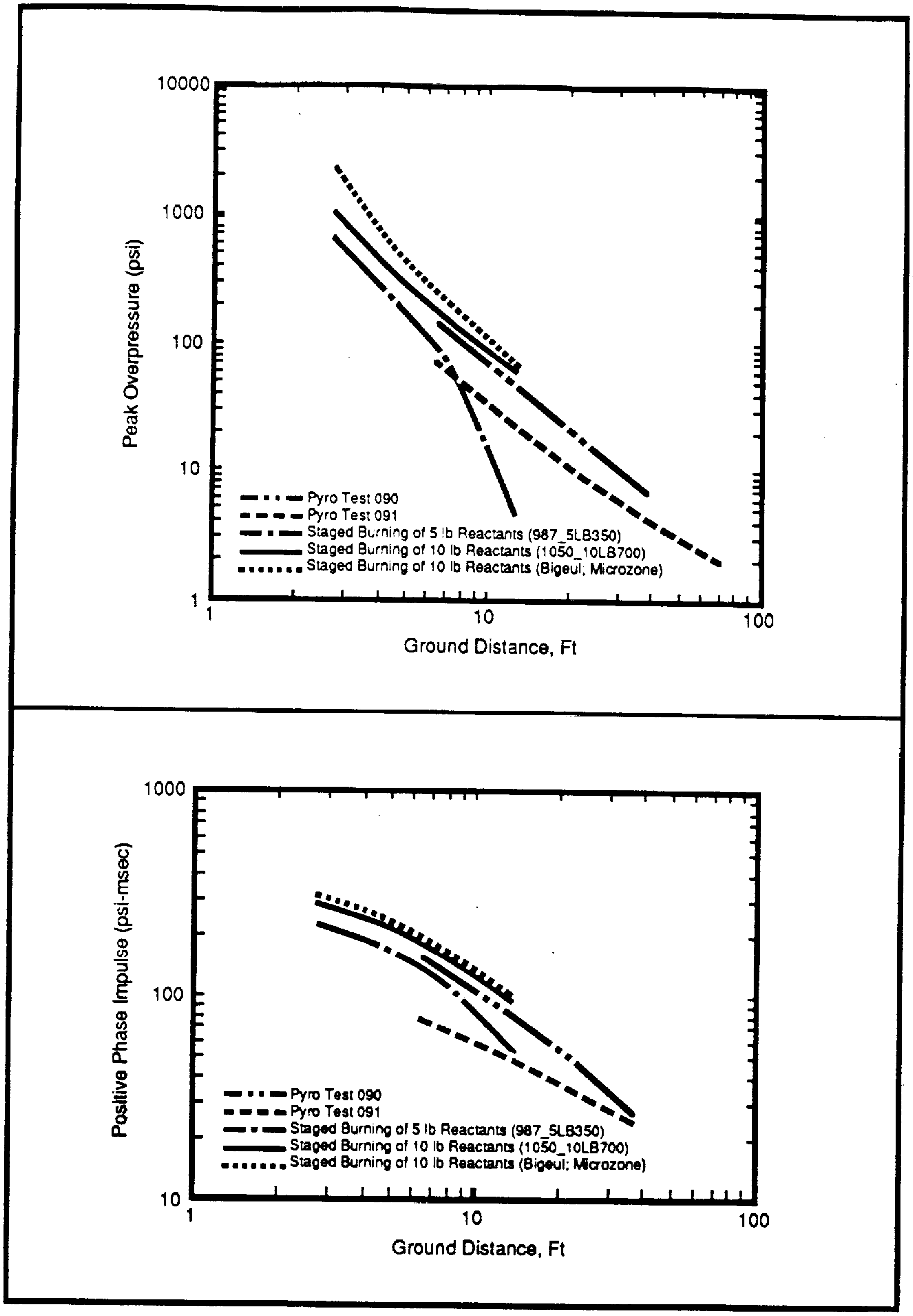

S-199.08C 12/89M

Figure 10. Comparison of Predicted and Measured Peak Overpressure and Impulse as a Function Distance from the Center of a 200 Lb. CBM Pyro Test.(1)

(1) Note that these values include the effect of height-of-burst

d. Refined Energy Addition Model Implications. A test of the hypothesis on which the refined energy addition model was based was required. This test was necessarily subjective. The test involved assessing the probability that the "core" and "surface" hydrogen could react with air in the time frame during which the energy addition was assumed to occur. Figures 11, 12, and 13 show the flow field developing around a ~200 lb PYRO-CBM type explosion with the energy addition staging shown in Figure 8. Careful examination of the location of the "core" hydrogen suggests that it is unlikely that any air will be available to react in the first 2.0 msec after the prompt reaction initiation. This is consistent with the assumption that there was no energy addition to the core hydrogen prior to 3.0 msec.

The "surface" hydrogen found air as soon as the prompt reaction ruptured the tankage. The outline of the surface hydrogen shown in Figure 13 suggests that the assumed rate of energy addition may be high for this material. It is clear that none of the unreacted hydrogen will react with the residual LO_2 since it is effectively walled off by the prompt-reaction products.

The results of the refined energy addition model calculations suggest that the explosive environment seen by an RTG located above a Centaur G' will not be similar to the environment in which the RTG components have been previously tested. It is likely that the RTG will be hit by a slug of unreacted liquid hydrogen in addition to the expected air and reaction product flow fields. The response of an RTG to an air and reaction product flow field was simulated in shock tube experiments conducted by Sandia and LANL personnel [8]. The impedance match between the gases and the simulated RTG does not provide for very efficient energy transfer in these experiments. It is expected that the reflected pressure produced by the impact of a slug of liquid hydrogen will be higher than that which is generated by a gas flow field of equal dynamic pressure. Determining how the impedance match between the liquid hydrogen and the RTG will affect the response of the GPHS plutonia contaminant system was beyond the scope of the present analysis.

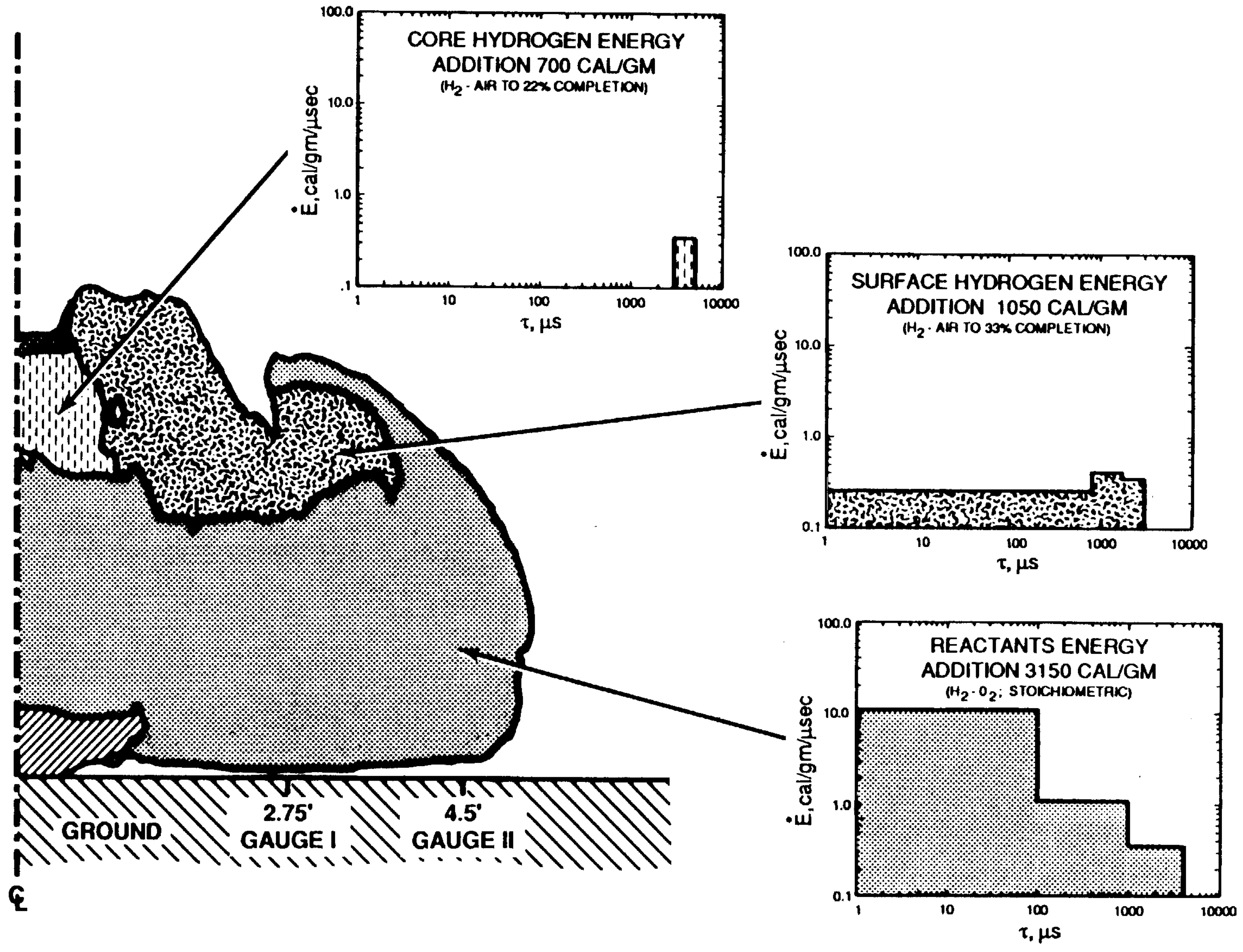

Figure 11. Pyro Test 90 and 91 Flow Field Simulation 840 μSec after Reactant Initiation. (10 lb. Reactants; 35 lb.LH_2; 180 lb. LOX)

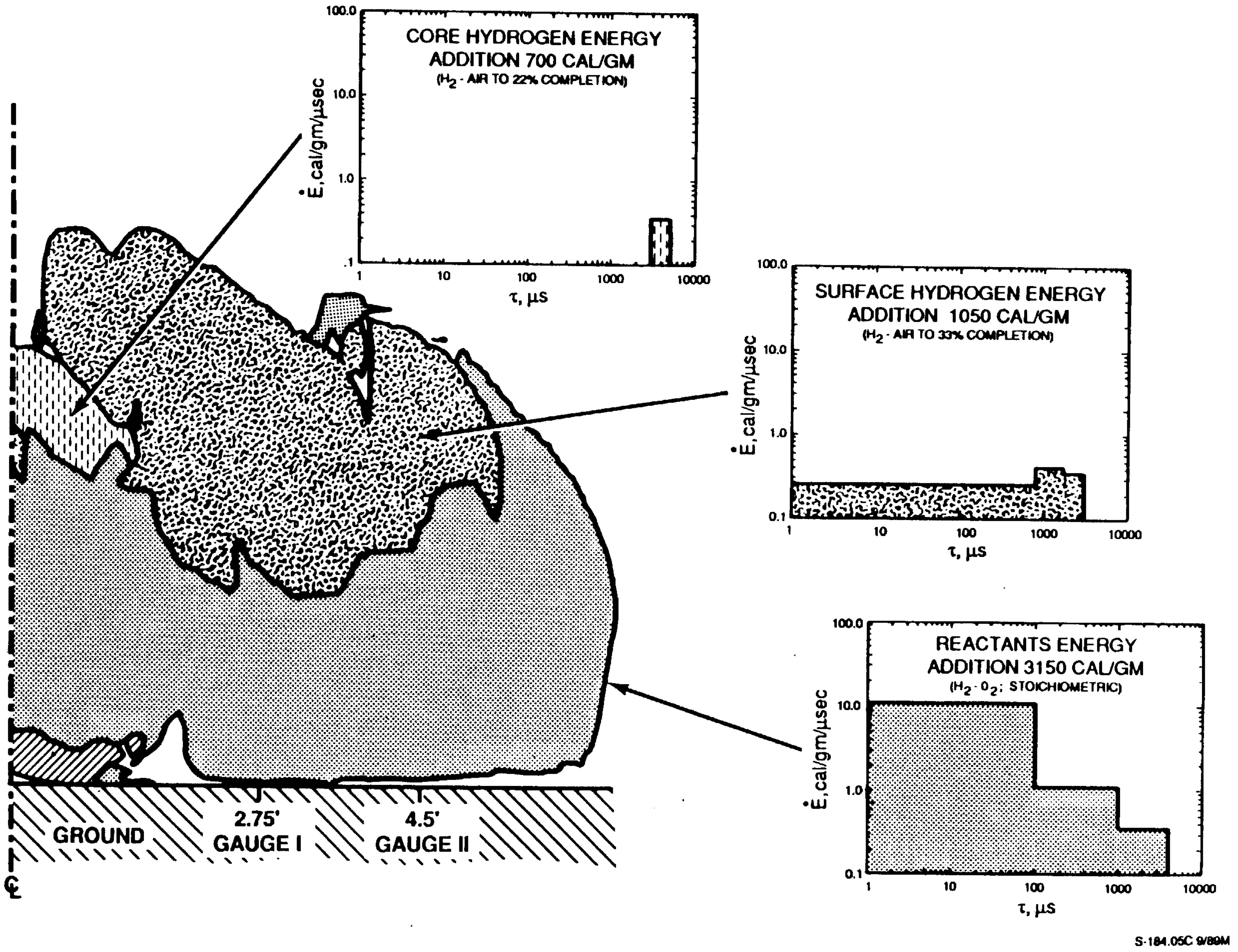

Figure 12. Pyro Test 90 and 91 Flow Field Simulation 1315 μSec after Reactant Initiation (10 lb. Reactants; 35 lb. LH_2;180 lb. LOX)

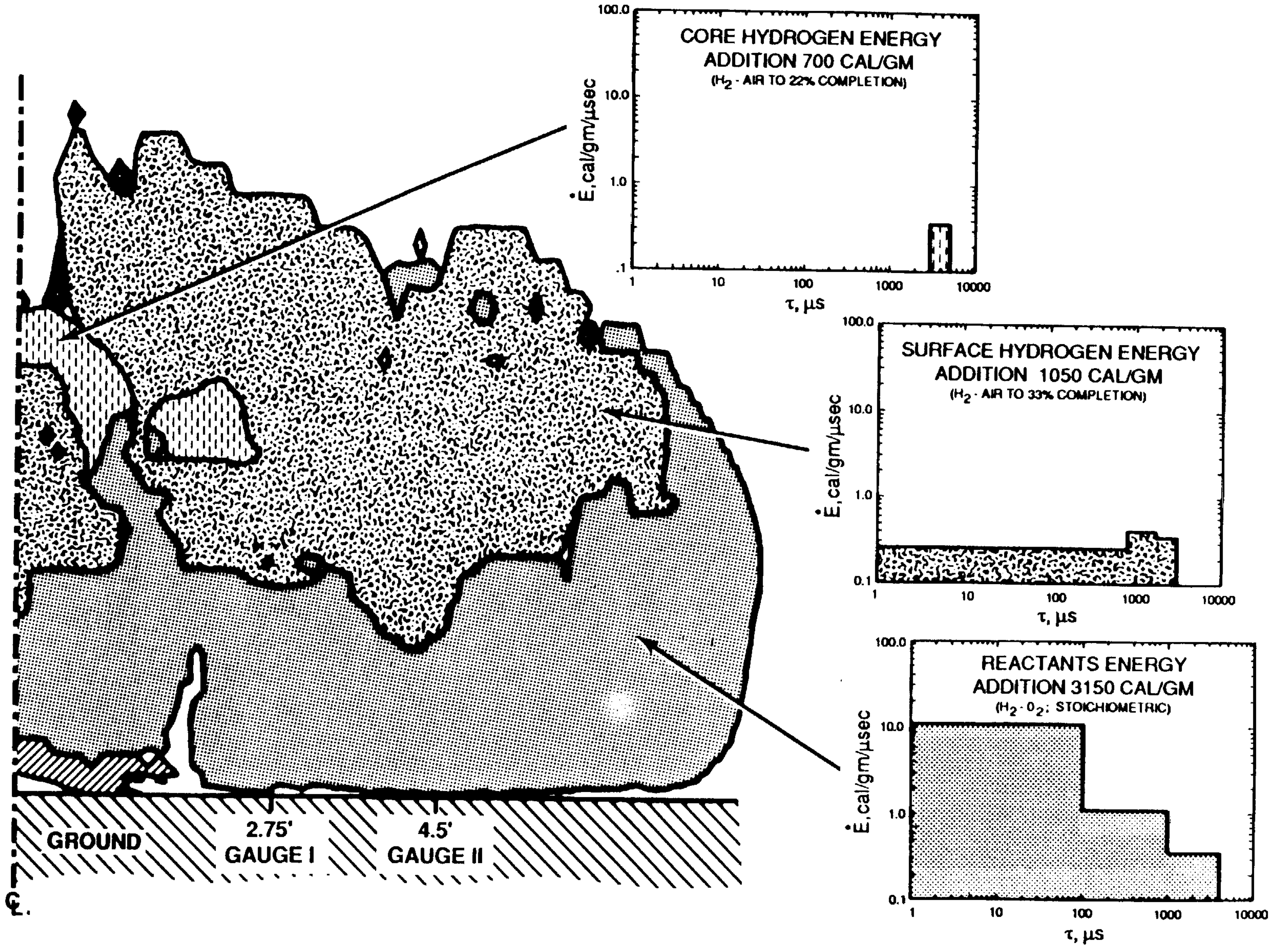

S-184.07C 9/89M

Figure 13. Pyro Test 90 and 91 Flow Field Simulation 1890 µSec after Reactant Initiation (10 lb. Reactants; 35 lb. LH_2;180 lb. LOX)

B. Environments Created by Centaur G' Explosions in the STS-Orbiter Bay

Prior to the STS-51L accident, the Galileo spacecraft was scheduled to be launched by an STS-Centaur G' combination. A number of calculations were performed to assess the range of environments to which the Galileo RTG might be subjected in the event of a Centaur G' explosion. However, use of a Centaur G' was disallowed after the STS 51L accident. This material is presented here for its archival value.

1. Analytical Model Description

An axisymmetrical coupled Eulerian-Lagrangian model having 1166 nodes was developed. A shell processor was used to simulate the STS wall while the cryogens were modeled in pure Eulerian coordinates. The cryogen tankage walls were not included in the model. Two phase equations-of-state were developed for the liquid cryogens using isentropic assumptions. The model was exercised over a range of potential explosive-environment boundary conditions to bound the possible values of static and dynamic pressures and impulses which could occur at the RTG location.

2. Analytical Model Geometry

The orbiter bay walls were modeled as an axisymmetric Lagrangian shell having an areal density of 0.603 gm/cm^2. The orbiter bay volume was modeled in the Eulerian coordinate system. The Euler grid was loaded with air at a pressure consistent with the altitude at which the Centaur explosion was assumed to occur (usually sea level and 75000 ft). Liquid hydrogen and liquid oxygen were loaded into an Eulerian grid in locations which approximated the geometry of the Centaur G' tankage.

Hydrogen and oxygen were assumed to mix in the oxygen tank ullage space. The degree of mixing (reactant density) and the reactant mass were limited by the volume available in the STS-Bay; i.e., the explosive reaction was assumed to initiate before the explosive mixture could diffuse outside of the orbiter bay. The general arrangement of the shells and reactants used in the analytical model is shown in Figure 14.

3. Analytical Model Parameters and Boundary Conditions

At the time that the subject calculations were performed, it had not been established that large amounts of liquid hydrogen-liquid oxygen mixing could not occur prior to the explosive initiation of the reactants. A number of experiments have since been performed to establish the density of the reactants which result from the mixing of liquid hydrogen and liquid oxygen. A range of densities was investigated to bound the potential environments which could result from such reactions. Cook and Udy [9] have suggested that explosive-reactant densities as high as 0.4 gm/cm could exist. Other investigators [10] hold that the results of Cook and Udy appear to be fading detonations from the strong initiators used in their experiments. Recent test-program results suggest that reaction densities of 0.0056 gm/cc are more representative of mixed LH_2-LO_2 reactions. A range of densities varying from 0.013 to 0.4 gm/cc was investigated in the study at hand. The results of one case with a charge density of 0.013 gm/cc are presented in detail because this density is the closest calculated to the 0.0056 gm/cc value observed in the mixing experiments.

For the purpose of these calculations, it was assumed that approximately 25 percent of the available reactants would mix prior to explosive initiation. It was shown previously (Section A) that perhaps only 2.5 to 5 percent of the available reactants were involved in the prompt yield measured in the PYRO-CBM experiments. In addition, several investigators [11, 5] have suggested that individual zones of 1000 lbs or more are unlikely to be found in explosions resulting from the mixing of liquid hydrogen and liquid oxygen. Further, experiments performed by Aerojet personnel [12] suggest that the amount of reaction mass available is controlled more by reactant contact area (tank aspect ratio) than by total reactant mass. For the above reasons, the reaction mass used in the subject calculations may be high by as much as an order of magnitude.

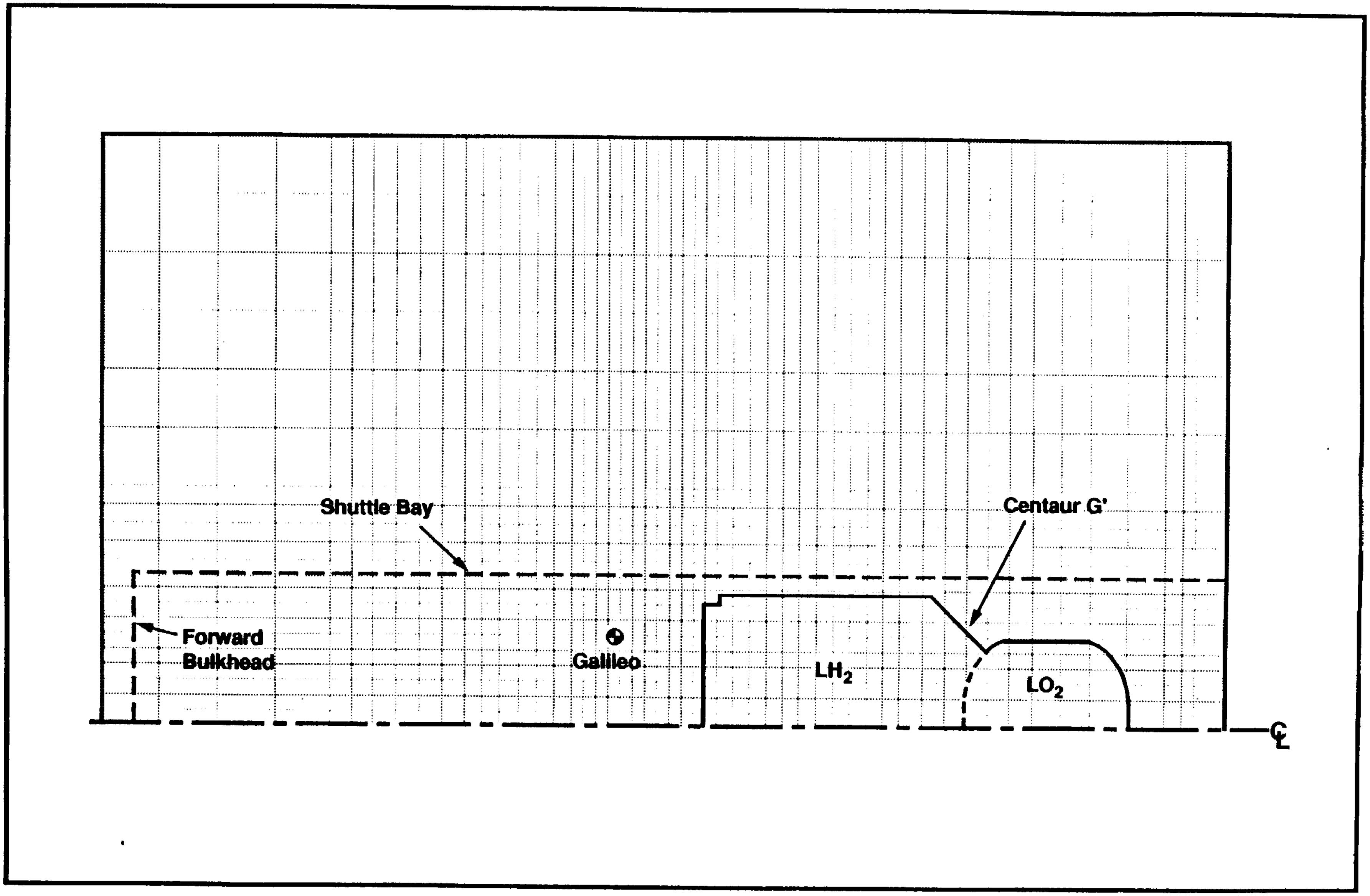

S-199.48C 8/90M

Figure 14. Initial STS-Centaur G' Geometry

The reaction energy resulting from LH_2-LO_2 explosions was a subject of considerable debate. It has been shown previously that two grossly different results can be obtained by assuming:

a) that the far field pressure and impulse may be range scaled $(W/L)^{1/3}$ to the near field, or

b) that the far field environment is primarily the result of hydrogen deflagration in air while the near field environment is the result of the detonation of a low density mixture of hydrogen and oxygen gas.

The calculations presented in this section are based on the assumption that various amounts of energy are added to 25 percent of the available reactants. The amount of specific internal energy added varied from 355 cal/gm to 3150 cal/gm. Energy was added to the reactants as a volume burn which occurred over a range of times. The burn time used varied from 20 to 400 microseconds. This range of burn times had no appreciable effect on the peak static or dynamic pressure resulting from the reaction.

The stocimetric reaction of hydrogen and oxygen releases 3150 cal/gm. It should be pointed out that the additions of lesser amounts of energy imply incomplete reaction of the available reactants. Thus, if one assumes 25 percent of the available mass reacts, and if one adds 1050 cal/gm to the reactants, the implication is that 8 percent (25 * 1050/3150) of the reactants actually burned. This method of bookkeeping reaction mass and energy appears awkward; however, some strategy of this type is necessary to account for the mass (inertia) of the unreacted reactants.

4. Analytical Predictions of Explosive Environments

The results of the eighteen parametric cases were analyzed. Five typical parametric calculations performed using the subject analytical model are summarized in Table III for the RTG location shown in Figure 14. Time histories of static and dynamic pressure and density

Table III. Flow Field Parameters at Galileo RTG Location(1)

CASE NUMBER	TEST INST	Y3554HP1	Y355RHP4	Y1050RHP1	Y1050RHP4
REACTION MASS, lbs	9766	9766	9963	9766	9963
REACTION DENSITY, g/cc	0.1	0.1	0.4	0.1	0.4
SPECIFIC ENERGY OF REACTION, cal/gm	355	355	355	1050	1050
BURN TIME, sec	20	400	400	400	400
MAX STATIC PRESSURE, bars	6.3	6.8	36	46	90
MAX Y-VELOCITY, m/sec	−200	−260	190	−460	880
MAX X-VELOCITY, m/sec	−400	−390	−760	−700	−1250
MAXX DENSITY, g/cc	.072	.072	0.73	0.74	0.74
MAX DYNAMIC PRESSURE, bars	56	57	190	175	600
STATIC IMPULSE, bar-sec	.023	.025	.045	.043	.078
DYNAMIC IMPULSE, bar-sec	.092	.092	.245	.215	.49

S-199.03L 12-89C

1) THE VALUES SHOWN ARE TIME-DEPENDENT. FOR EXAMPLE, PEAK STATIC AND DYNAMIC PRESSURES DO NOT OCCUR AT THE SAME TIME. SEE LOCATION TIME HISTORY FIGURES FOR DETAILS.

at this same location are presented in Figure 15. Examination of this figure leads to the conclusion that the postulated explosion has the effect of accelerating a large slug of liquid hydrogen into the RTG. This phenomenon is especially evident in the time-history of density shown in the last panel of Figure 15. Note that the density of liquid hydrogen is .07145 gm/cc. One can see from this Figure the time at which the LH_2 front arrives at the RTG location and the duration of passage of the LH_2 slug.

Figure 16 shows the flow field which develops as a result of the explosion of reactants having a charge density of 0.1 gm/cc in the Centaur G' LO_2 ullage. The development of an air shock followed by the high density reaction products, followed by the passage of the LH_2 slug is clearly indicated by the vectors and the pressure contours shown in these plots. Figures 17 and 18 show the development of the flow field resulting from a similar reaction except the charge density has a value of 0.013 gm/cc, which more closely approximates the experimentally observed density.

5. Implication of Analytical Predictions

The Centaur G' explosion flow fields predicted by the available analytical models are considerably different from those assumed to exist by the RTG proof test designers. It is clear that the threat to the RTG is not that of a blast wave such as was generated in the DOE-conducted shock tube tests. Rather, it is the response generated by the impact of tank fragments, avionics boxes, a column of LH_2 and the implosion of the RTG housing if it resides in a reactant gas environment. The response to these environments must be evaluated for RTGs stored close to LH_2 tankage. To the authors' knowledge, no program to assess such a response has been conducted to date.

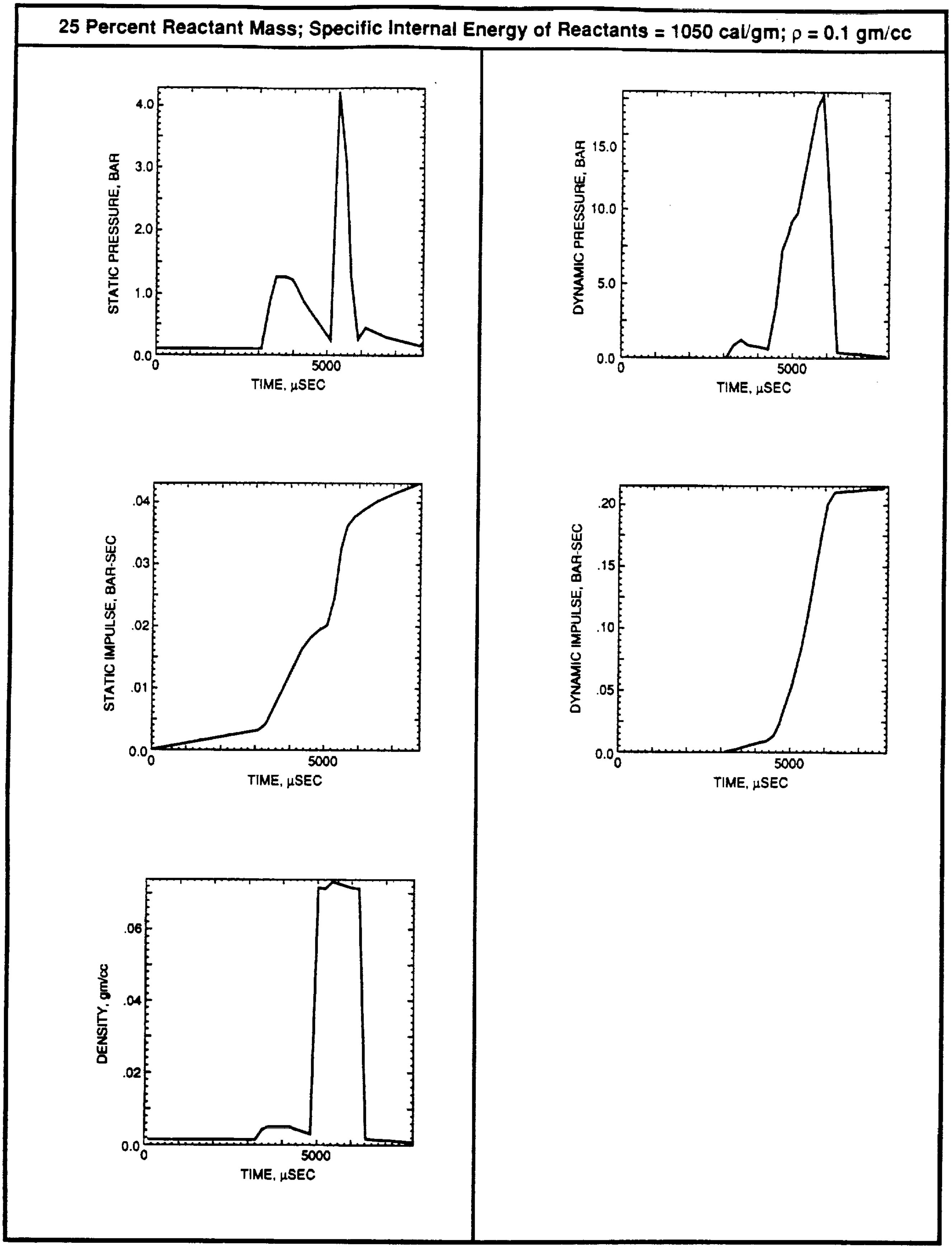

25 Percent Reactant Mass; Specific Internal Energy of Reactants = 1050 cal/gm; ρ = 0.1 gm/cc

S-199.17C 8/90M

Figure 15. Time Histories of the Flow Field Environment at the Galileo RTG Location in the STS-Bay.

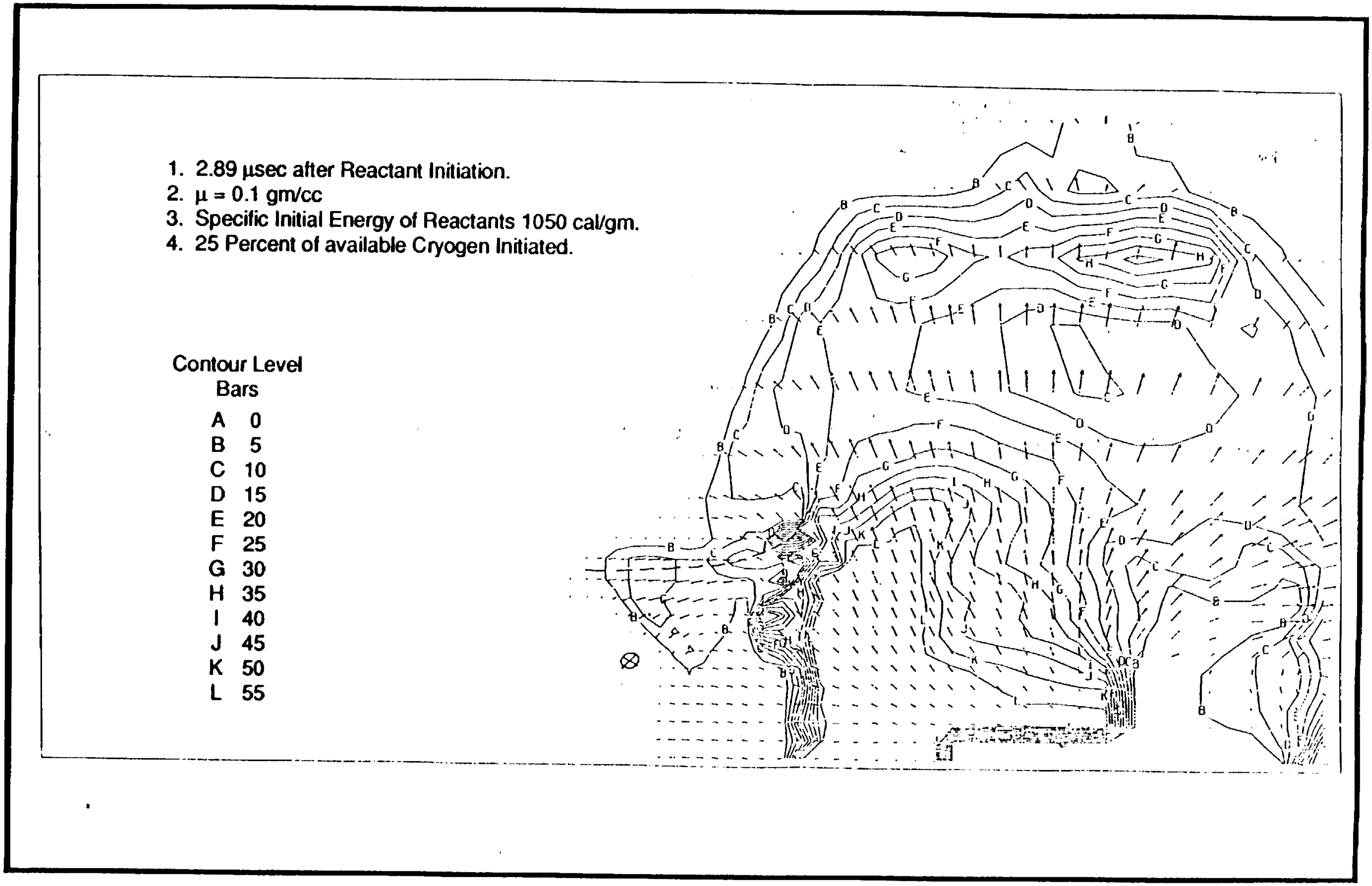

1. 2.89 µsec after Reactant Initiation.
2. µ = 0.1 gm/cc
3. Specific Initial Energy of Reactants 1050 cal/gm.
4. 25 Percent of available Cryogen Initiated.

Contour Level	Bars
A	0
B	5
C	10
D	15
E	20
F	25
G	30
H	35
I	40
J	45
K	50
L	55

S-199.18C 12/89M

Figure 16. Flow Field Developing in the STS Bay following an Explosion in Centaur G' LOX Ullage.

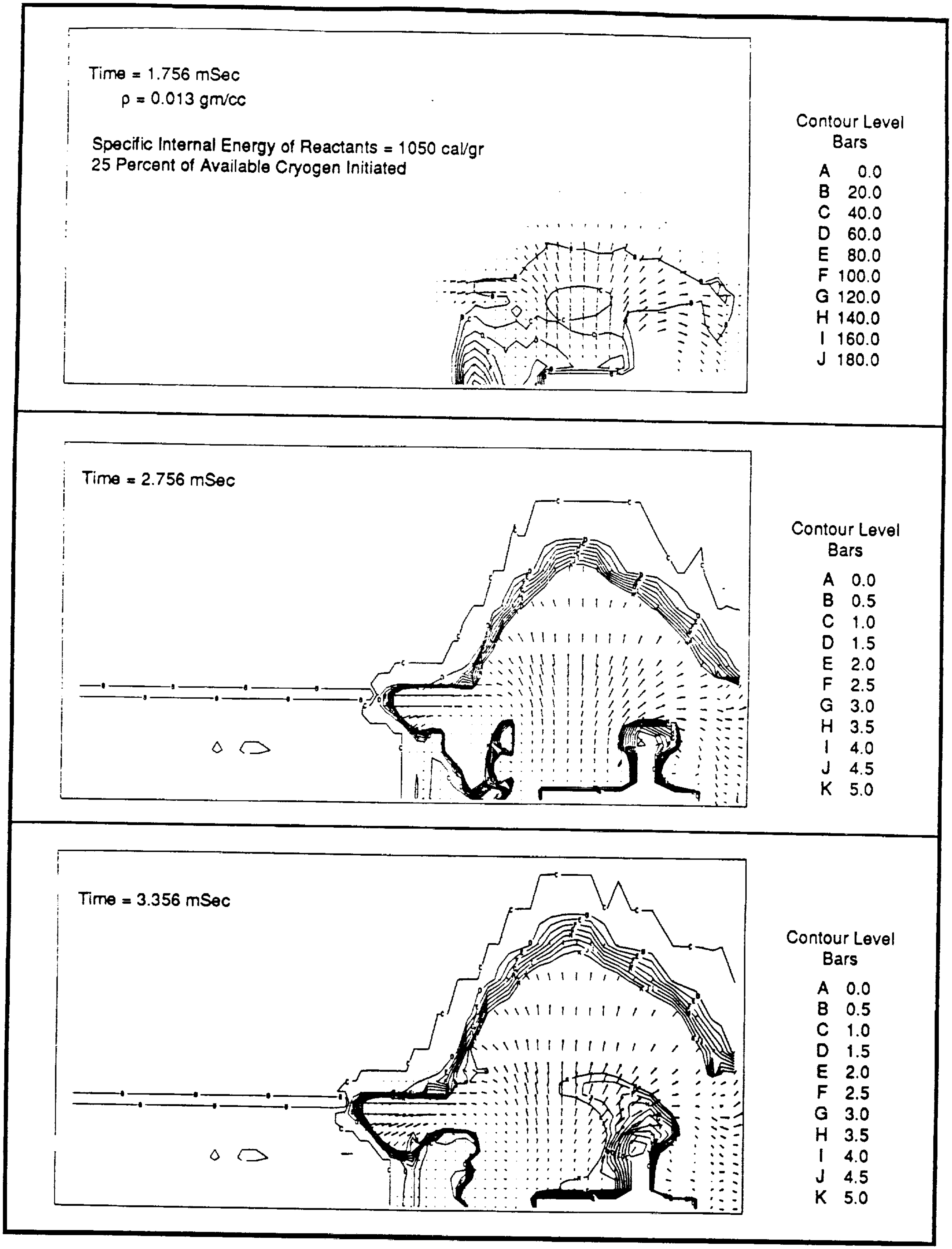

Figure 17. Flow Field Developing in STS Bay Following an Explosion in the Centaur G' LOX Ullage. (Con't)

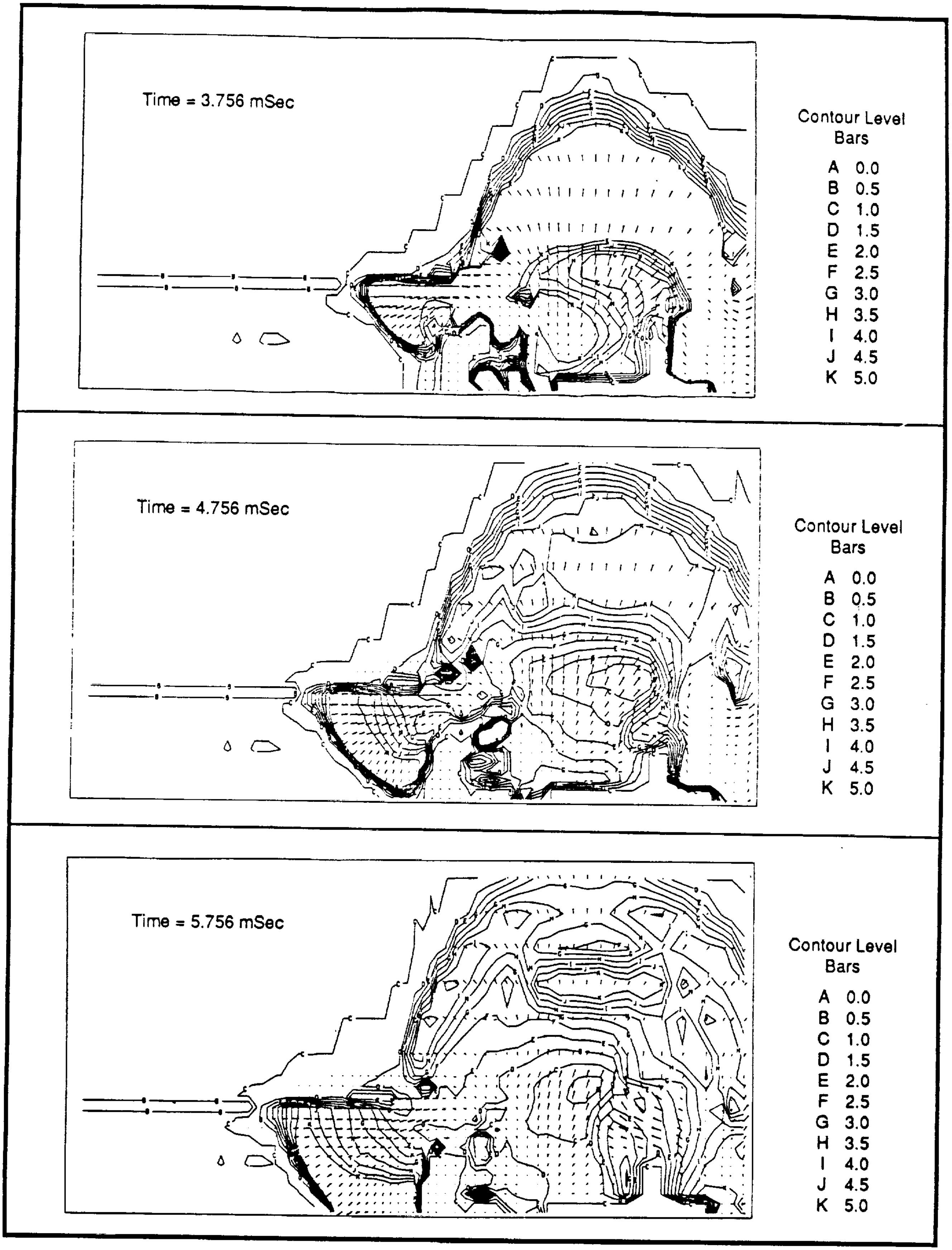

S-199.20C 12/89M

Figure 18. Flow Field Developing in STS Bay Following an Explosion in the Centaur G' LOX Ullage. (Con't)

C. Environments Created by the Expansion of Liquid Cryogens into Vacuum Absent Explosion

Detailed calculations were conducted to assess the potential hazard within the STS-Bay involved in the expansion of liquid cryogens in the absence of reaction energy addition. The model simulated the STS-Bay using a Lagrangian shell processor while the cryogens were simulated in Eulerian coordinates using equations-of-state which assumed isentropic expansion of the stored cryogen when their normal storage pressure was dropped to the pressure consistent with an altitude of 70000 feet.

1. Summary

Sudden depressurization of a liquid cryogen will cause the formation of vapor bubbles within the liquid, and vaporization from the liquid free surface. The rate of the liquid free surface expansion is determined by the rate of vapor bubble nucleation and growth. The driving force for vapor bubble nucleation and growth is the difference between the liquid temperature and the temperature corresponding to the local saturation pressure. Expansion of the vapor leaving the free surface is retarded by surface tension and its own inertia. Bubble growth is retarded by surface tension, the bubble vapor inertia, and the inertia of the liquid surrounding the vapor bubble.

The complex interaction between the thermodynamic driving force and inertial restraining force was modeled in axial symmetry and Eulerian coordinates. The equation of state used for the liquid hydrogen implies zero time for bubble nucleation and isentropic expansion of the vapor, i.e., the work done by the vapor as it accelerates itself and the surrounding liquid is reversible [13]. These assumptions lead to the highest possible equilibrium expansion velocities. Equilibrium thermodynamic calculations show that the internal energy available to cause liquid expansion is only 18 cal/gm. Once this energy is removed, the liquid will be at the freezing temperature. The volume change associated with freezing is small and further expansion due to vapor formation cannot occur.

Particle velocities of 600 meters/sec were calculated for molecules leaving the free liquid surface. These high velocity molecules do no damage to structure because the density of their flow field is very low, and even though very high particle velocities are calculated, the associated dynamic pressures are very low. As a result, no structural damage is caused by the initial high velocity flow field. As the expansion continues, the RTG is immersed in a two-phase froth containing roughly 11 percent vapor. The peak dynamic pressure associated with the flow of this froth is ~0.58 bar. A dynamic pressure of this magnitude will not damage the RTG housing.

Comparisons of the expansion of LH_2 into vacuum with the expansion of water into vacuum are appropriate; however, great care must be taken to correct for differences in the equations of state, internal energy and the inertial behavior of the two fluids. Project High Water released water to space at an altitude of 165 km. The temperature of this water (i.e., internal energy available to drive the expansion) must be known to assess the applicability of the observed results. In addition, the dynamic pressure developed by the water expansion must be known before the destructive effects of that expansion can be assessed. Damage estimates based on water vapor particle velocity alone are inappropriate.

2. Model Description and Results

The time zero axisymmetrical model geometry may be inferred from examination of Figure 22 where an STS-Bay wall areal density of 0.609 gm/cm^2 was used. The expansion of LH_2 saturated at a pressure of 20 psia was tracked for 100 milliseconds after complete tankage failure occurred. The dynamic pressure at the RTG location was calculated to be 8.4 psi. This is well below the threshold of damage for the RTG. There was, of course, no air shock. These results are not surprising since liquid hydrogen has very little internal energy to provide an energetic driving force.

Brief descriptions of the model assumptions and the underlying thermodynamic principles are presented in the following discussion.

The dependence of vapor pressure on the temperature of liquid normal hydrogen is presented in Figure 19. The specific heat of liquid hydrogen as a function of temperature is presented in Table IV. The equation of state (EOS) used in the PISCES code analyses is shown in Figure 20. This EOS is an upper bound of the available driving force for fluid mass acceleration because it assumes:

1) An equilibrium tracking of the Hugoniot in the liquid phase.
2) Isentropic expansion in the vapor phase.
3) Zero time for vapor volume nucleation and growth.

The expansion of a liquid into a vacuum involves the lowering of the temperature of the residual liquid in order to provide the heat required to generate vapor. This is another way of saying that the vapor is in thermal equilibrium with the residual liquid as the local static pressure is reduced to the terminal expansion pressure. The terminal expansion is the end of the expansion process. In the absence of internally deposited energy, the only heat available to the process is that stored in the liquid at a temperature greater than the saturation temperature corresponding to the terminal expansion pressure. Reference to Figure 19 shows that the temperature of liquid hydrogen saturated at 20 psia is 21K. Liquid hydrogen is in equilibrium with solid hydrogen at 14K.

The usual method of solution for this type of problem is to refer to a T-S diagram and expand the fluid along an isentrope. This is what was done in generating the reference EOS. It may be useful to introduce a less elegant conceptual approach to explain the analyzed environment.

Consider a gram of liquid hydrogen saturated at 20 psia (21K). The average specific heat (C_p) over the range 21K to 14K is approximately 2.5 cal/gm, K. The energy available to accelerate the mass of liquid and gaseous hydrogen which forms on the instantaneous and total removal of the LH_2 tank wall may be calculated as follows:

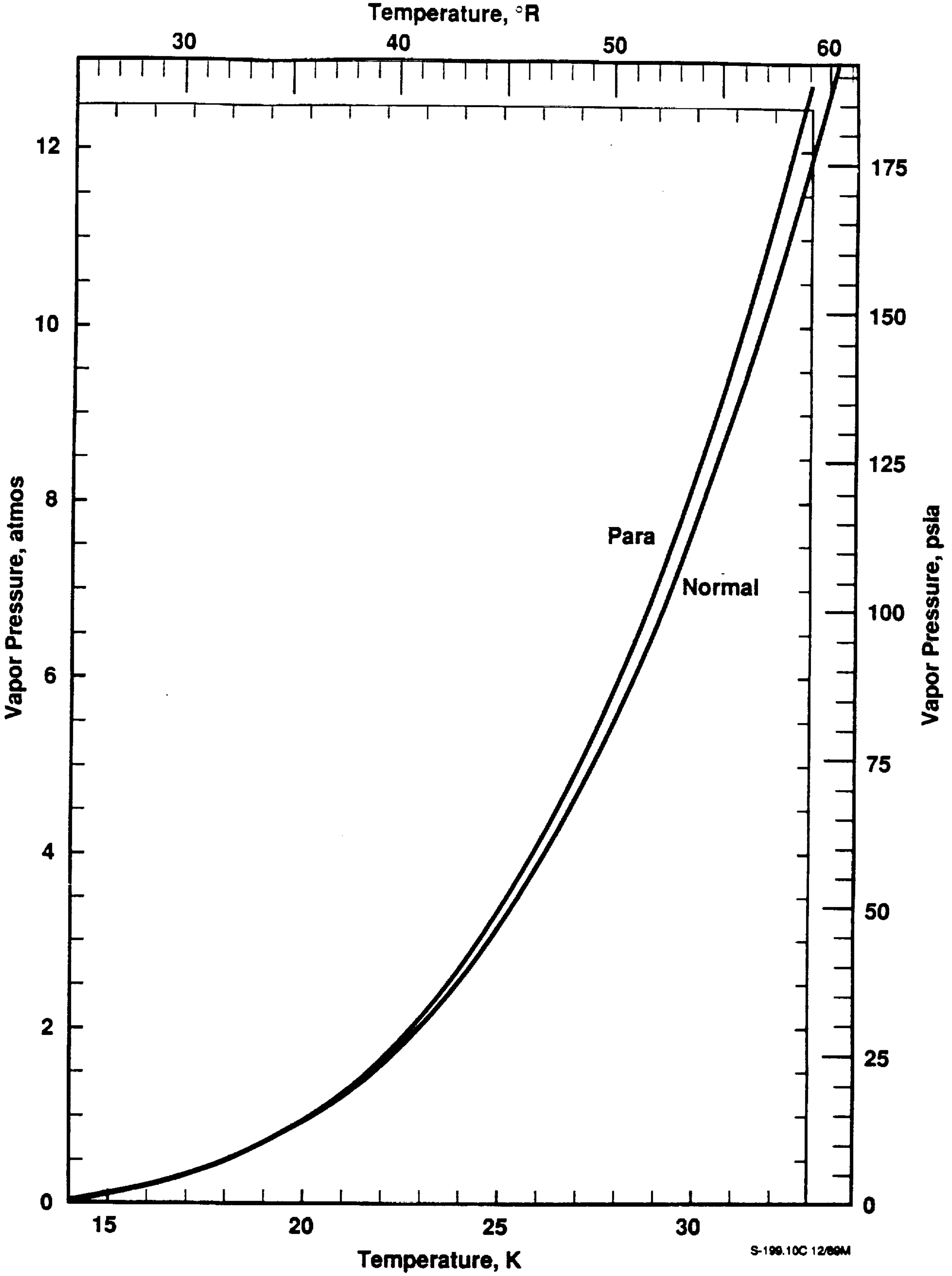

Figure 19. Vapor Pressure of Liquid Hydrogen (Normal and Para)

Table IV. Specific Heats (C_p and C_v) of Normal Hydrogen Gas

	0 ATM			1 ATM		
TEMP (K)	k	C_p cal/g/K	C_v cal/g/K	k	C_p cal/g/K	C_v cal/g/K
20	1.667	2.4643	1.478			
30	1.667	2.4643	1.478	1.736	2.5904	1.492
40	1.666	2.4653	1.480	1.700	2.5274	1.487
50	1.664	2.4692	1.484	1.684	2.5067	1.489
60	1.658	2.4830	1.498	1.672	2.5076	1.500
70	1.646	2.5106	1.525	1.655	2.5283	1.528
80	1.628	2.5540	1.569	1.634	2.5678	1.571
100	1.583	2.6752	1.690	1.587	2.6831	1.691
120	1.539	2.8162	1.830	1.541	2.8211	1.831
140	1.502	2.9502	1.964	1.503	2.9532	1.965
160	1.474	3.0636	2.078	1.475	3.0665	2.079
180	1.454	3.1582	2.172	1.455	3.1602	2.172
200	1.439	3.2331	2.248	1.439	3.2351	2.248
220	1.427	3.2923	2.307	1.428	3.2933	2.306
240	1.419	3.3386	2.353	1.419	3.3396	2.353
260	1.413	3.3751	3.389	1.413	3.3761	2.389
270	1.410	3.3889	2.403	1.410	3.3899	2.404
280	1.408	3.4007	2.415	1.408	3.4017	2.416
300	1.405	3.4194	2.434	1.405	3.4204	2.434

S-199.04C 8-90C

Source of Data:

Hilsenrath, J., et al., NBS Cir. 564 (1954), 282.

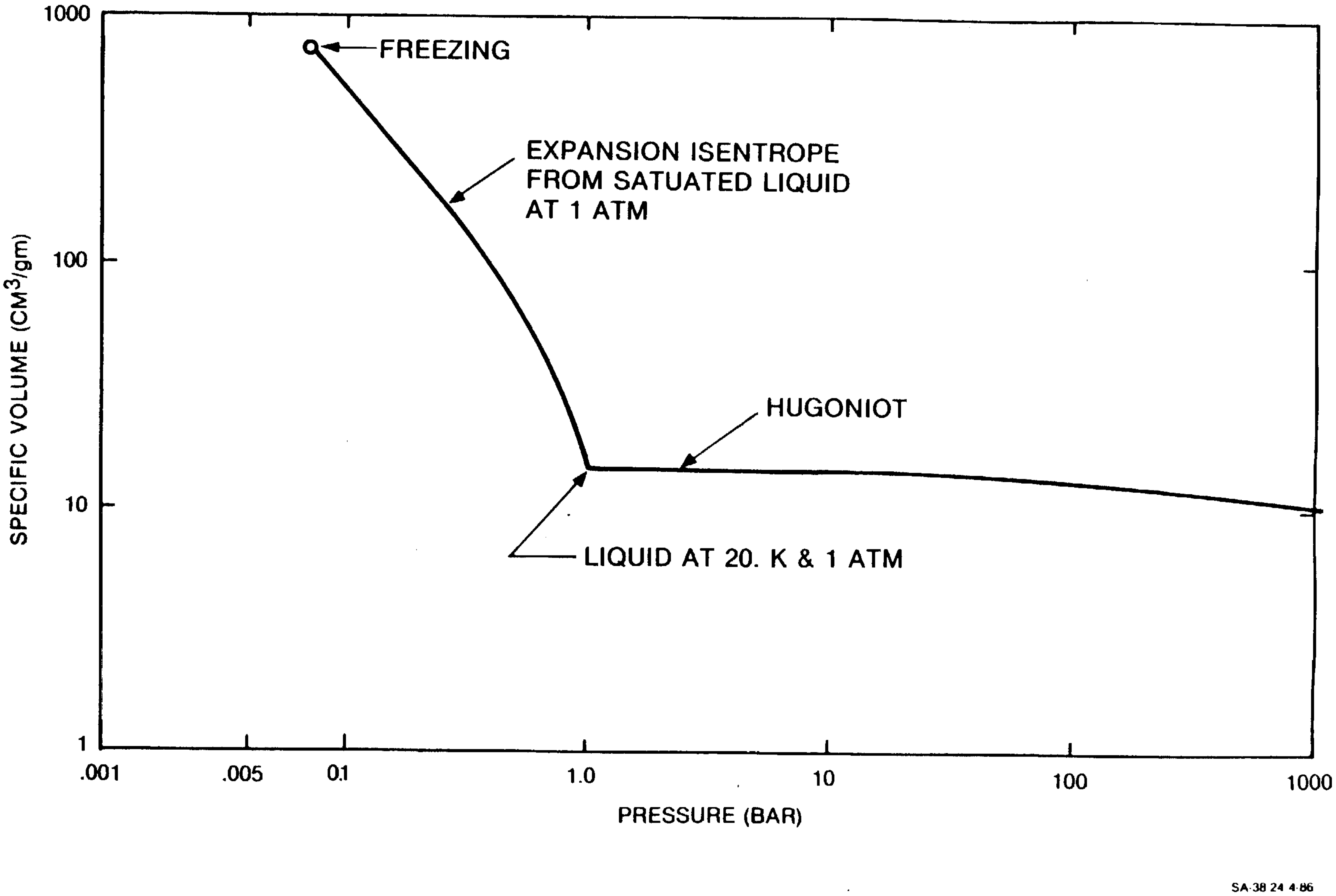
FREEZING
EXPANSION ISENTROPE
FROM SATUATED LIQUID
AT 1 ATM
HUGONIOT
LIQUID AT 20. K & 1 ATM
1000
100
10
1
SPECIFIC VOLUME (CM^3/gm)
.001
.005
0.1
1.0
10
100
1000
PRESSURE (BAR)
SA-38 24 4-86

$$Q/W = C_p (T_s - T_f) \qquad (1)$$

where:

Q/W = Available specific energy, cal/gm
C_p = Specific heat, cal/gm K
T_s = Saturation temperature at 20 psia, K
T_f = Freezing temperature, K

Although one may make the argument that solid hydrogen will sublime in vacuum, it seems reasonable to limit the lower energy availability level to the freezing temperature. Substituting the data quoted from Table IV and Figure 19 into equation (1) we see that the maximum available specific energy is 17.5 cal/gm. Even if this energy were available independent of rate of removal, which it is not, this would not constitute a very energetic explosion. Given this low specific energy availability, it is not surprising that the RTG is predicted to undergo little disturbance.

Figure 21 provides the information to deduce the nature of the expanding hydrogen flow field at the initial RTG location. Figure 22 shows the flow field pressure contours and velocity vectors within the STS Cargo Bay and in the immediate vicinity of the RTG for various times after tankage failure. The heavy dashed line in Figure 22 indicates the position of the Cargo Bay doors at the indicated time. The circumscribed x shows the initial location of the RTG. Note that the problem is axisymmetric. There is no leakage indicated through the doors. The pressure contours shown above the heavy dashed lines are an artifact of the plot routine. This routine plots the average pressure within an Euler cell at the center of the cell having the next higher row number than the shell boundary. As a result, some of the pressure contours appear to move through the STS doors. Careful examination of the vectors shown on these same figures shows that there is no flow through (orthogonal to) the STS wall in the region of interest. Although the particle velocities shown are very high, the density in this region is very low. As a result, there is no effect on the environmental traces at the RTG location.

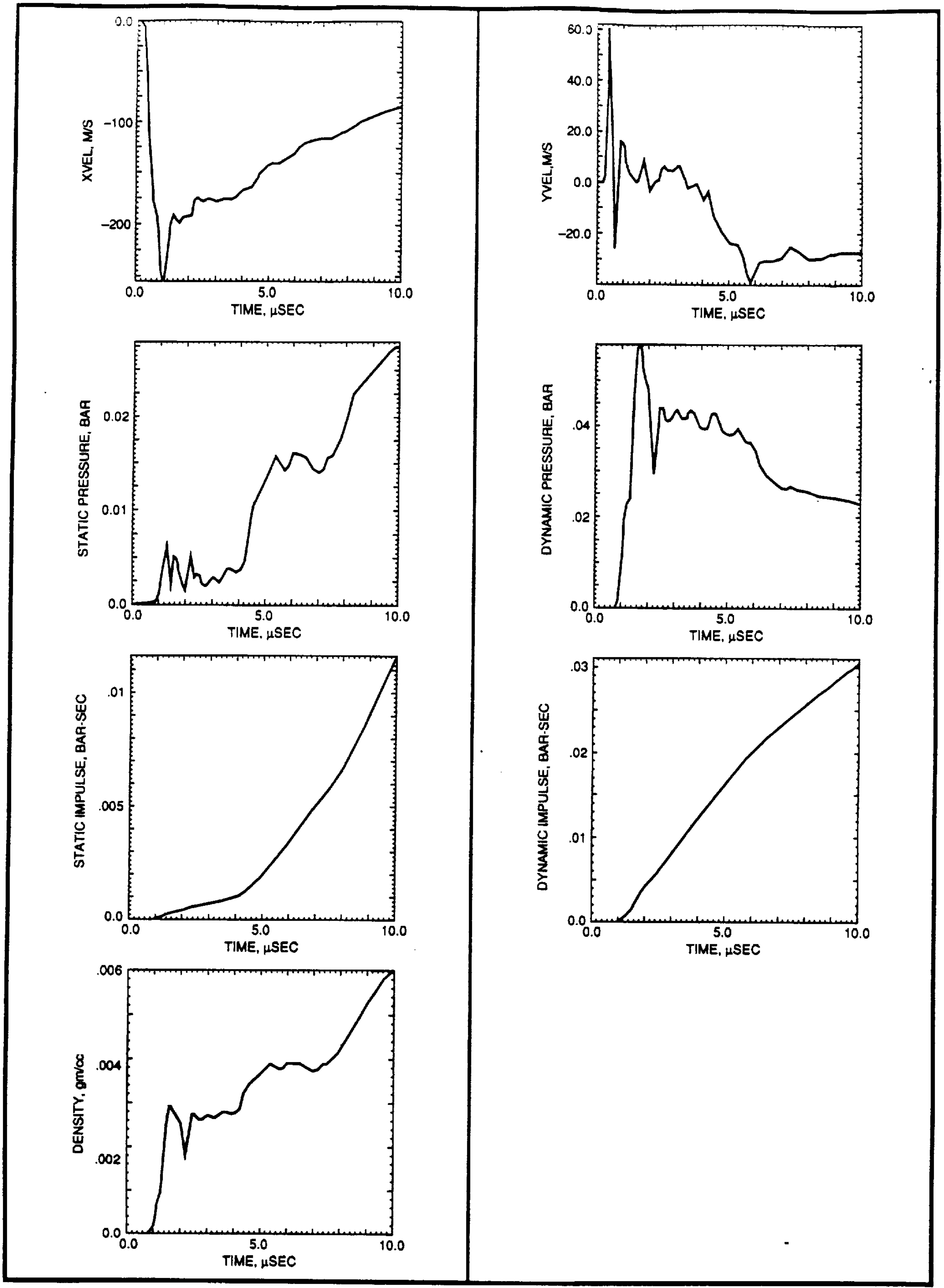

S-199.21C 6/90M

Figure 21. Time Histories of the Flow Field Environment at the Galileo RTG Location in the STS-Bay following the Failure of the Centaur G' Tankage with No Explosion.

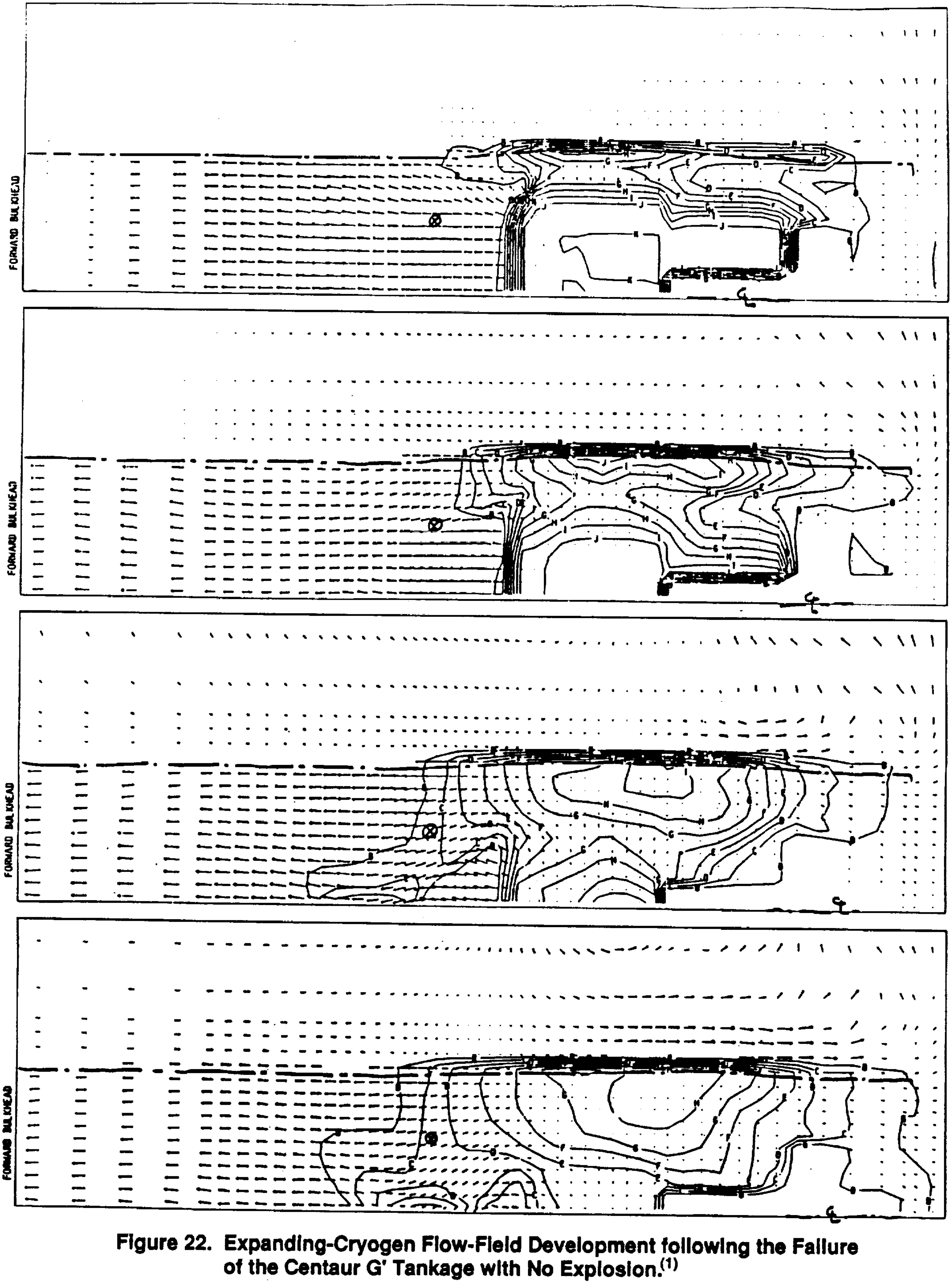

Figure 22. Expanding-Cryogen Flow-Field Development following the Failure of the Centaur G' Tankage with No Explosion.[1]

[1] Galileo RTG location shown by ⊗

D. Environments Generated by a Centaur G' Explosion under a Titan IV Shroud

Considerable work was done to establish the environment which would result from the explosion of a Centaur G' under a Titan IV Payload Fairing (PLF). This work produced results similar to results obtained in the study of Centaur G' explosions in the STS-bay. This work was also used as the basis for the Centaur Initiated Bulkhead Failure environments presented in the Titan IV data book [4]. Through out the remainder of this section, reference will be made to environments at both the Galileo and CRAF RTG locations under the PLF. The CRAF location results were the basis of a Monte Carlo analysis which was used to assess the probabalistic blast environments.

A description of the Titan IV-Centaur G' bulkhead failure explosion model as well as predicted environments and the probability of their occurrence are presented in the following paragraphs. The underlying uncertainties in these environments are discussed.

1. Analytical Model Description

The Centaur G' model is identical to that described in Section B.1. The major differences in the overall model arise from the geometry and areal density differences in the STS-Bay walls and the Titan IV PLF. The Centaur G' is again modeled in pure Euler with no tankage walls. The Euler nodes are loaded with cryogens to simulate their time-zero location. The remainder of the Euler grid is loaded with air having standard atmospheric conditions at an altitude of either sea level or 70000 feet. The Euler grid contains 1166 nodes with an average cell dimension of 15 cm in the region of interest. A graphical representation of the analytical model is presented in Figure 23.

2. Model Boundary Conditions

The input to the analytical model was specified by JPL personnel. Ranges of reactant density of 0:0056 to 0.4 gm/cc were investigated. Staged burning of the reactants was investigated. The reactant energy addition profile shown in Figure 6 was used. No LH_2

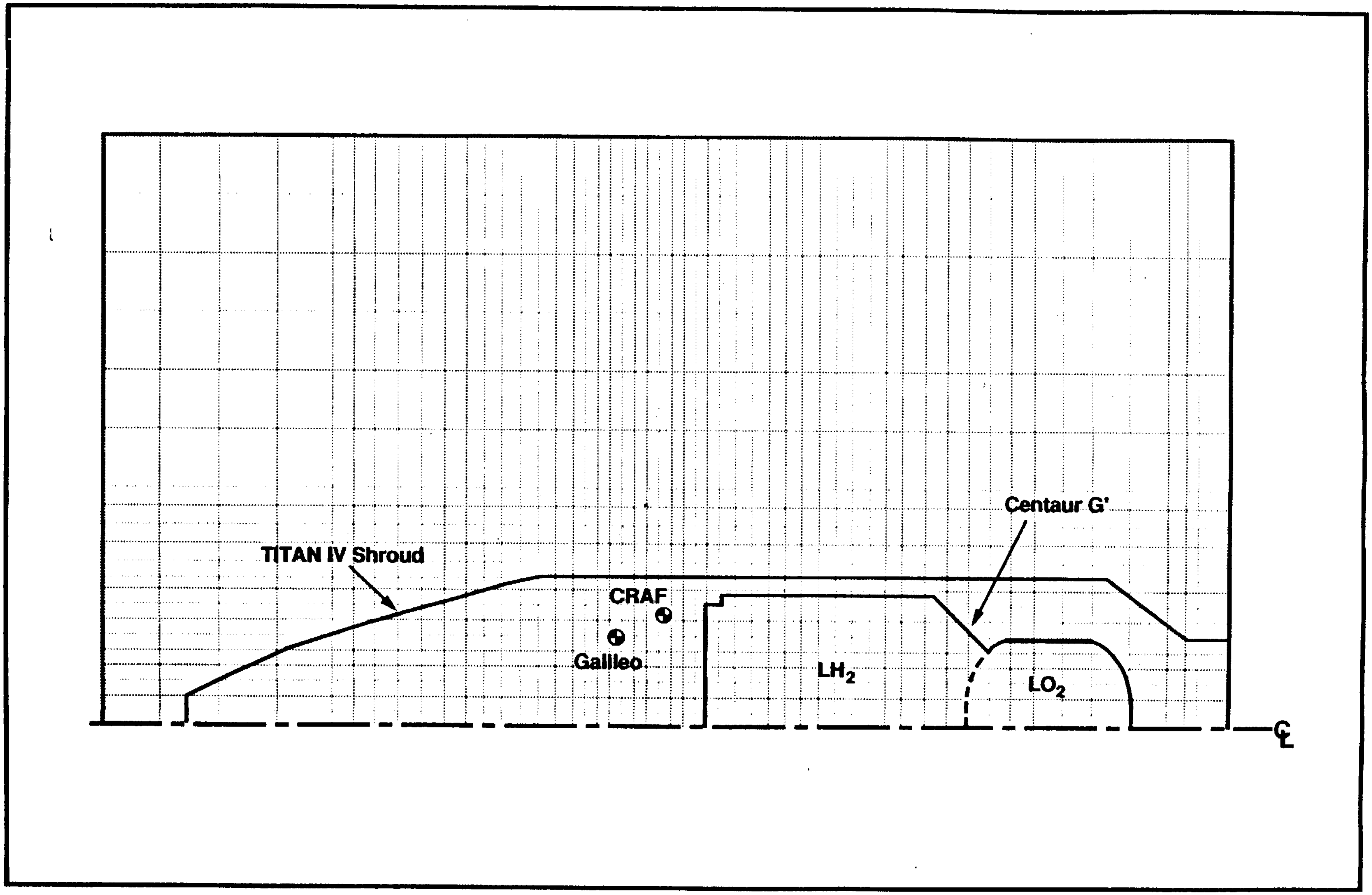

S-199.27C 6/90M

Figure 23. Initial Titan IV Shroud - Centaur G' Geometry

vaporization and after burning was considered. A range of prompt reaction mass was studied. This range varied from ~1 to ~5 percent (472 to 2306 pounds) of the available propellant mass.

The location of the reactants at the time of initiation is a significant driver in the low-reactant-density explosion cases. Initial studies showed that there were significant variations in possible positions of the reactants following a tankage failure and prior to explosion initiation. Low charge density results in minimal acceleration of the liquid hydrogen slug. If most of the LH_2 is present and the explosion occurs in the LO_2 ullage, the flow fields at the CRAF or Galileo RTG locations have a trivial effect on the RTG. A parametric study of the effect of reactant location on the environment at the RTG location was conducted. The parametric locations of the reactants relative to the LH_2 and LO_2 are shown for a number of 0.013 gm/cc charge density cases in Figure 24. As in the case of the STS-bay calculations, it was assumed that the PLF would contain the reactants prior to initiation. This assumption has the effect of limiting the available cross sectional area of the charge face. Similar geometry limitations were observed for charge length and charge depth.

Two specific charge-geometry-development scenarios were used to determine the time zero charge geometries shown in Figure 24. Both conserve the available Centaur G' and Titan IV shroud volume. It was assumed in scenario A, that a leak developed in the common bulkhead between the LH_2 and LO_2 tanks. Further, it was assumed that this leak went undetected and the the higher pressure LO_2 flowed into the LH_2 tank evaporating much of the LH_2 which was expelled into the atmosphere through the Centaur PLF overboard vent system. The effect of this scenario is to reduce the shielding effect of the LH_2 mass. The reaction mass was assumed to occupy the appropriate volumes of the LH_2 tankage and LO_2 ullage for the purpose of these calculations.

The second postulate (Figure 24, scenario B) was that the reactant mass developed as a result of a common bulkhead failure due to loss of LO_2 pressurization. In this scenario, the LH_2 falls by pressure difference and gravity into the LO_2 ullage, spills over the side of the tank LO_2 and remains confined by the Titan IV shroud.

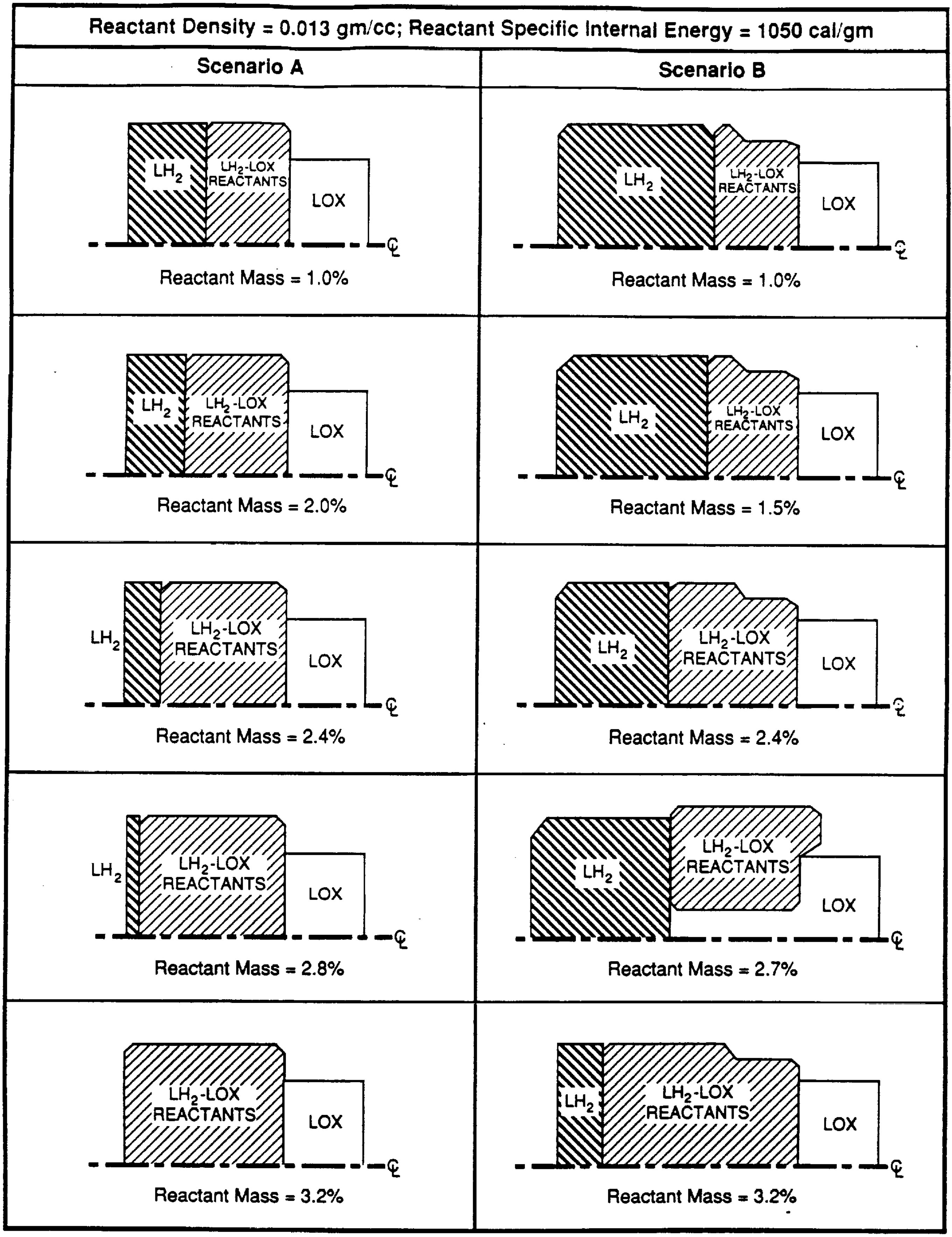

Figure 24. Time-Zero Cryogen Locations for Two Assumed Centaur G' Tankage-Failure Scenarios.

A third and, most probable scenario, is that the gaseous hydrogen which is generated by mixing of LH_2 with LO_2 after a loss-of-pressurization common bulkhead failure will mix with air and/or gaseous oxygen, fill the volume under the Titan IV shroud and initiate. The resultant gas explosion would surround the RTG and tend to implode it. The consequences of such an explosion would not be serious if the reactant gases raise to nominal atmospheric temperature before detonation because the maximum pressure which can result from a GH_2-GO_2 explosion is approximately 900 psia. This pressure is far below the 2000 psia to which the GPHS modules were tested in the shock tube experiments. If the reactant gas temperature is close to that of the saturated liquid cryogens, and if they mix in a stoichiometric, ratio, the detonation pressure could be greater than 3000 psia. No calculations using gaseous density reactants enveloping the RTG were performed; however, it may reasonably be concluded that all possible steps should be taken to preclude the possibility that the RTG will be immersed in a cold gas detonation region.

3. Analytical Results

Selected results from the parametric study which investigated initial (Scenarios A and B) reactant geometry are shown in Table V. Examination of this Table shows the strong shielding effect provided by the unreacted LH_2 mass. It should be noted, however, that the peak dynamic pressures are not greatly different.

Snapshots of the developing flow field following the explosion of the Centaur G' cryogens are presented in Figure 25. The mass of the LH_2 causes the reaction products to flow primarily radially from their Scenario B location. A spherical blast wave which engages the RTG develops with time. Even after 25 msec, the LH_2 mass is essentially a continuous body. A general assessment of the nature of the flow field can be made by studying the flow vectors and comparing the mass location plots to the pressure contour plots. The strong gradients shown in the pressure contour plots develop because of reflections from the cryogen liquid surfaces and the Titan IV shroud.

Table V. Comparison of Flow Field Characteristics at the Galileo and CRAF Locations

DATA SET NAME	OVER PRESSURE, BAR		DYNAMIC PRESSURE, BAR		STATIC IMPULSE, BAR-SEC		DYNAMIC IMPULSE, BAR-SEC		MASS OF REACTANTS LBS
	CRAF	GALILEO	CRAF	GALILEO	CRAF	GALILEO	CRAF	GALILEO	
SCENARIO A INITIAL GEOMETRY									
RP013__F4P0	9.0	4.35	12.4	11.4	0.010	0.018	0.067	0.063	2297
RP013__F4P1	33.0	20.5	140.0	190.0	0.078	0.058	0.065	0.104	1876
RP013__F3P2	10.4	29.0	43.8	46.5	0.021	0.024	0.082	0.090	1478
RP013__F2P7	8.30	7.30	11.20	8.0	0.0245	0.0260	0.043	0.055	1280
RP013__F2P4	2.85	2.25	14.75	14.25	0.0069	0.0069	0.057	0.056	1079
RP013__F1P0	3.25	3.00	2.45	2.1	0.0108	0.0128	0.014	0.00335	472
RP013__F1P5	4.60	3.80	4.60	4.5	0.0155	0.0165	0.0415	0.042	681
SCENARIO B INITIAL GEOMETRY									
RP013__4P0X	32.5	20.0	152.5	195.0	0.080	0.060	0.072	0.074	2306
RP013__F3P2X	32.50	29.0	33.0	52.0	0.084	0.080	0.059	0.060	1476
RP013__F2P4X	9.0	8.0	56.0	60.0	0.021	0.016	0.080	0.086	1079
RP013__F1P5X	7.20	6.0	13.0	13.0	0.016	0.018	0.064	0.062	681

S-199 01C 8-90C

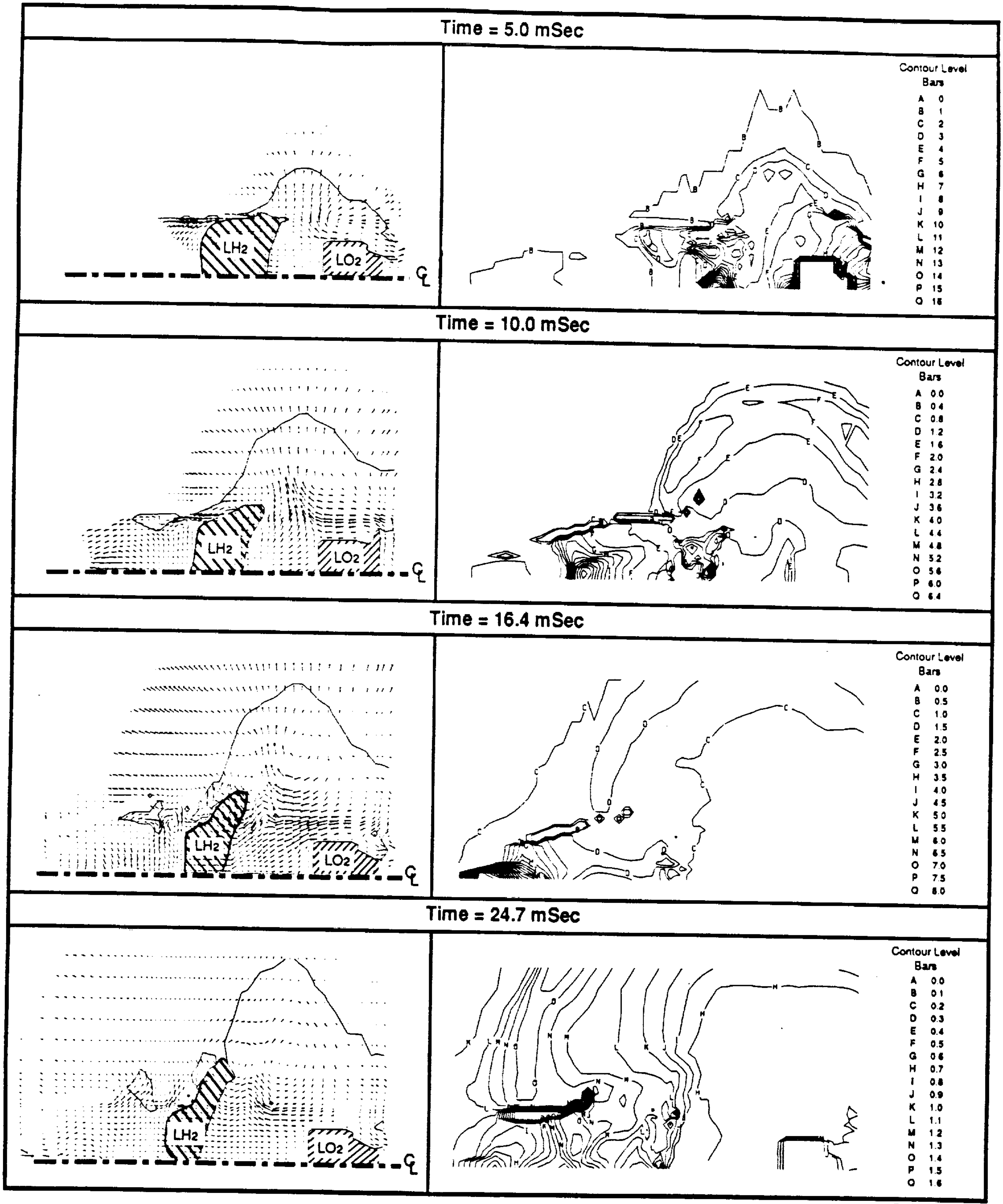

Figure 25. Flow Field Development following the Explosive Reaction of Centaur G' Cryogens using Scenario B Initial Geometry.

ρ = 0.013 gm/cc Reactant Mass = 472 lbs. Specific Internal Energy of Reactants = 1050 cal/gm

A detailed comparison of the explosive environments developed in the 0.013 gm/cc density Scenario A and Scenario B cases may be made by examining Figures 26 and 27. These figures show that a slug of liquid hydrogen passes the RTG location between 8 and 12 mSec after initiation given the Scenario A initial reactant geometry. The LH_2 has not arrived at the RTG location after 30 msec because of its greater mass in the Scenario B initial geometry. The Scenario B results were not used in the subsequent Monte Carlo calculations because the environments they described were so benign.

4. Monte Carlo Analysis

A matrix of cases having the characteristics of those described in Section D was run. The initial conditions for three cases were varied to cover the range of reactant physical properties and locations which were thought to be reasonable. The results of these calculations are presented in Table VI. Note that, with some exceptions, the environment at the RTG location tends to become more severe as reactant density and mass increase. The exceptions to this general rule are caused by complex interactions between the reactant mass and the residual LH_2 mass. Choice of initial reactant location is not always topologically consistent given that there are a large number of possible reactant configurations for the lower mass-higher density cases.

The results presented in Table VI are shown graphically in Figures 28 and 29. Note that the mass fractions are truncated when the product of reactant mass and density reaches the total available volume within the Centaur hydrogen tank and oxygen ullage volumes (1955 ft^3).

A Monte Carlo analysis was performed using the analytical results presented in Table VI (furnished by JPL) and the probability distribution functions described in Table VII. These input probability density functions presented in Table VII were input to a statistical random number generator routine in order to draw random samples of mass fraction and density of reactants.

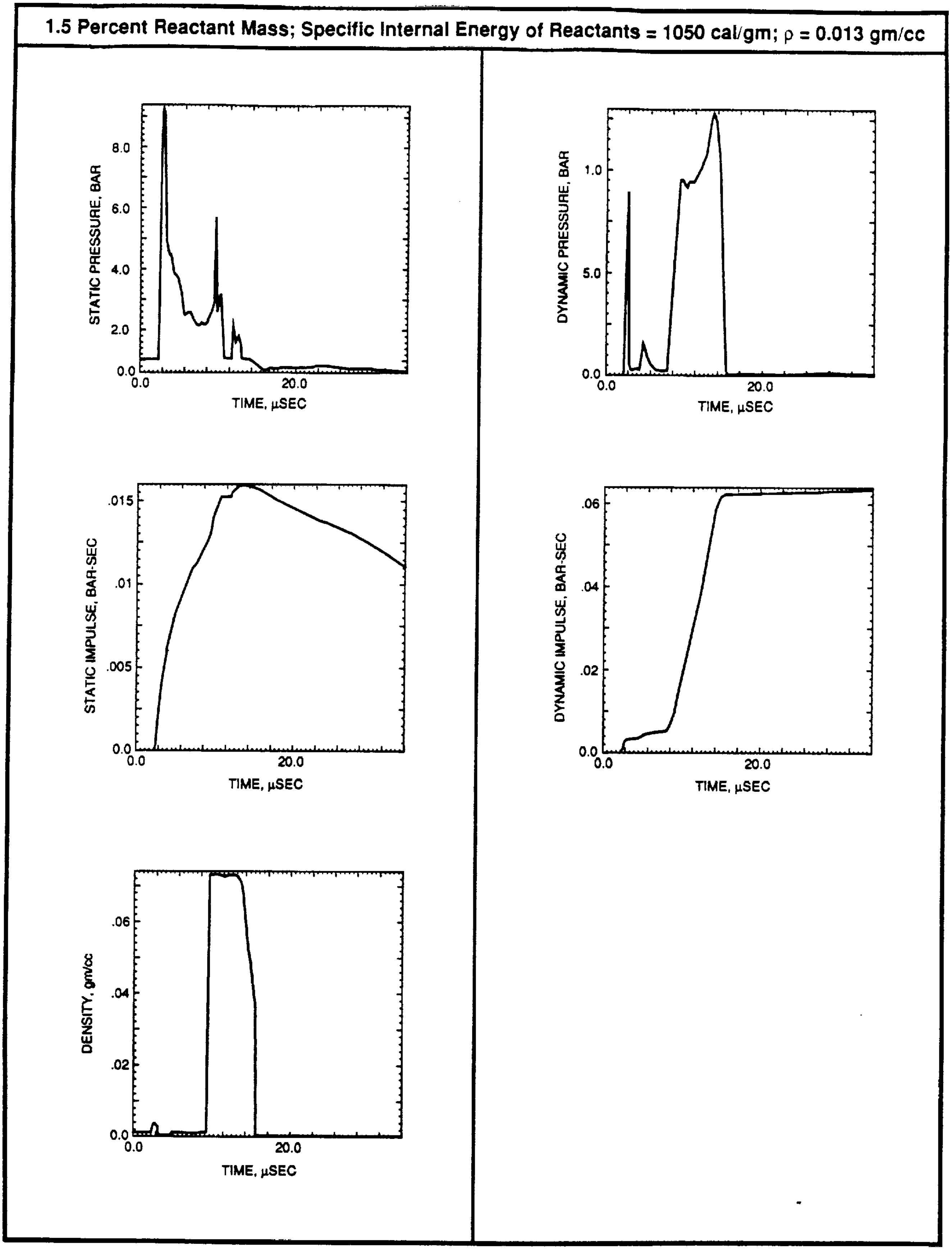

1.5 Percent Reactant Mass; Specific Internal Energy of Reactants = 1050 cal/gm; ρ = 0.013 gm/cc

S-199.15C 6/90M

Figure 26. Details of the Flow Field Environment at the CRAF Location following a Scenario A Explosion of the Centaur G' for Case RP013_F1P5X

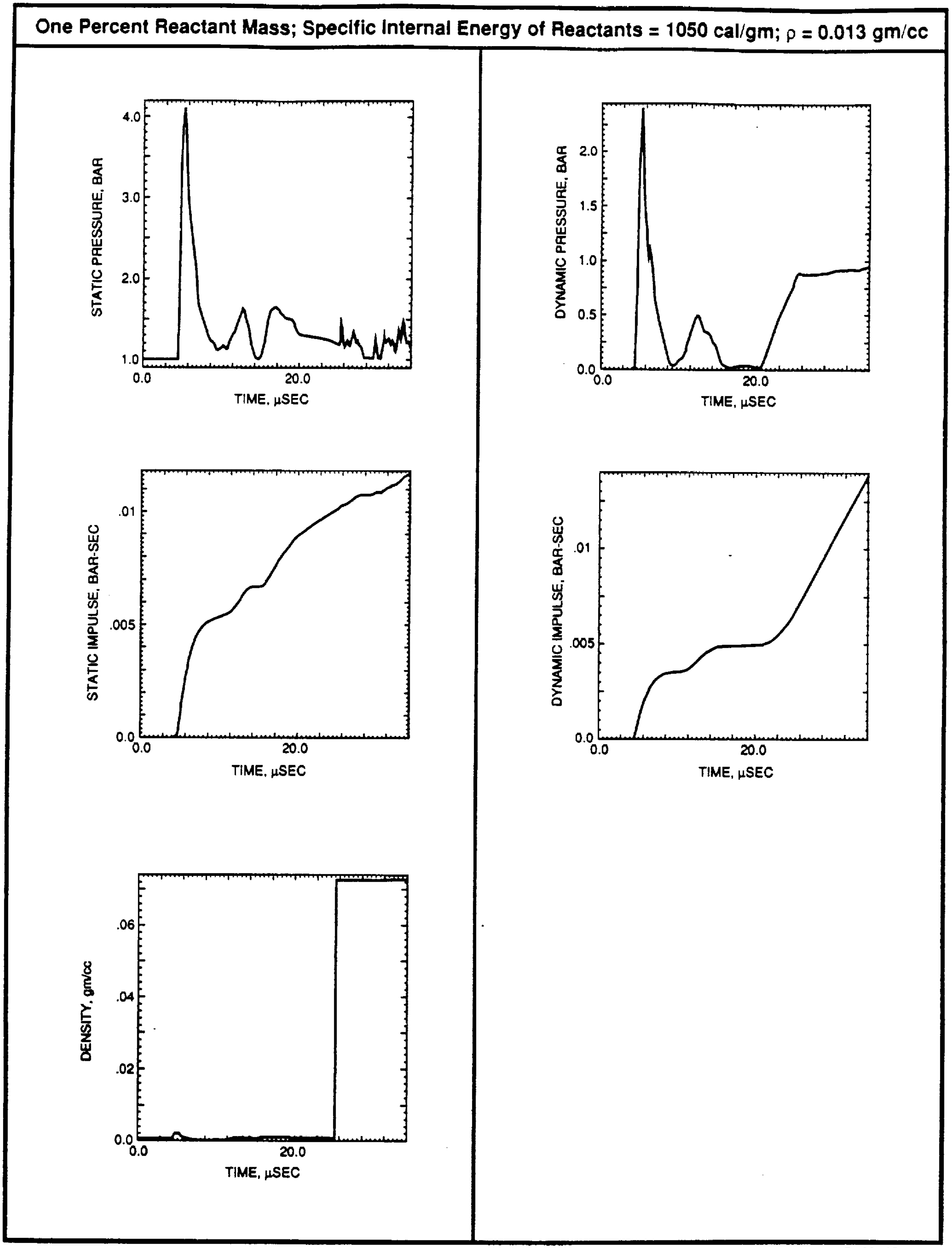

One Percent Reactant Mass; Specific Internal Energy of Reactants = 1050 cal/gm; ρ = 0.013 gm/cc

S-199.16C 6/90M

Figure 27. Details of the Flow Field Environment at the CRAF Location following a Scenario B Explosión of the Centaur G' for Case RP013_F1P0

Table VI. CRAF Location Flow Field Environments Predicted for a Number of Assumed Reactant Conditions

1050 cal/gm Prompt and Reactant Only Staged Energy Addition Assumed

Density g/m^3	Mass Fraction %	Static Pressure PSI	Dynamic Pressure PSI	Static Impulse PSI-SEC	Dynamic Impulse PSI-SEC
.0056	0.75	68.2	68.2	.203	0.60
	1.20	101.5	181.3	.261	0.76
	1.60	268.3	210.3	.870	0.36
.013	1.5	104.4	188.5	.232	0.93
	2.0	116.0	464.0	.232	1.12
	2.4	130.5	812.0	.305	1.16
	2.8	478.5	2755.0	.783	1.16
	3.2	471.3	478.5	1.218	0.86
.026	1.4	78.3	127.6	.128	0.725
	2.4	41.3	174.0	.123	0.899
	3.0	92.8	253.8	.136	1.073
	4.8	253.8	594.5	.392	1.160
.050	1.7	58.0	188.5	.203	0.841
	2.8	116.0	391.5	.247	1.305
	3.7	101.5	435.0	.145	1.392
	4.8	116.0	638	.218	1.595
0.1	1.3	100	271	.161	.911
	2.0	74	199	.152	.703
	3.5	155	587	.283	1.305
	4.8	216	1160	.370	161
04	0.8	130	435	.166	.841
	9.0	319	899	.305	1.42

S-199.24C 1-90C

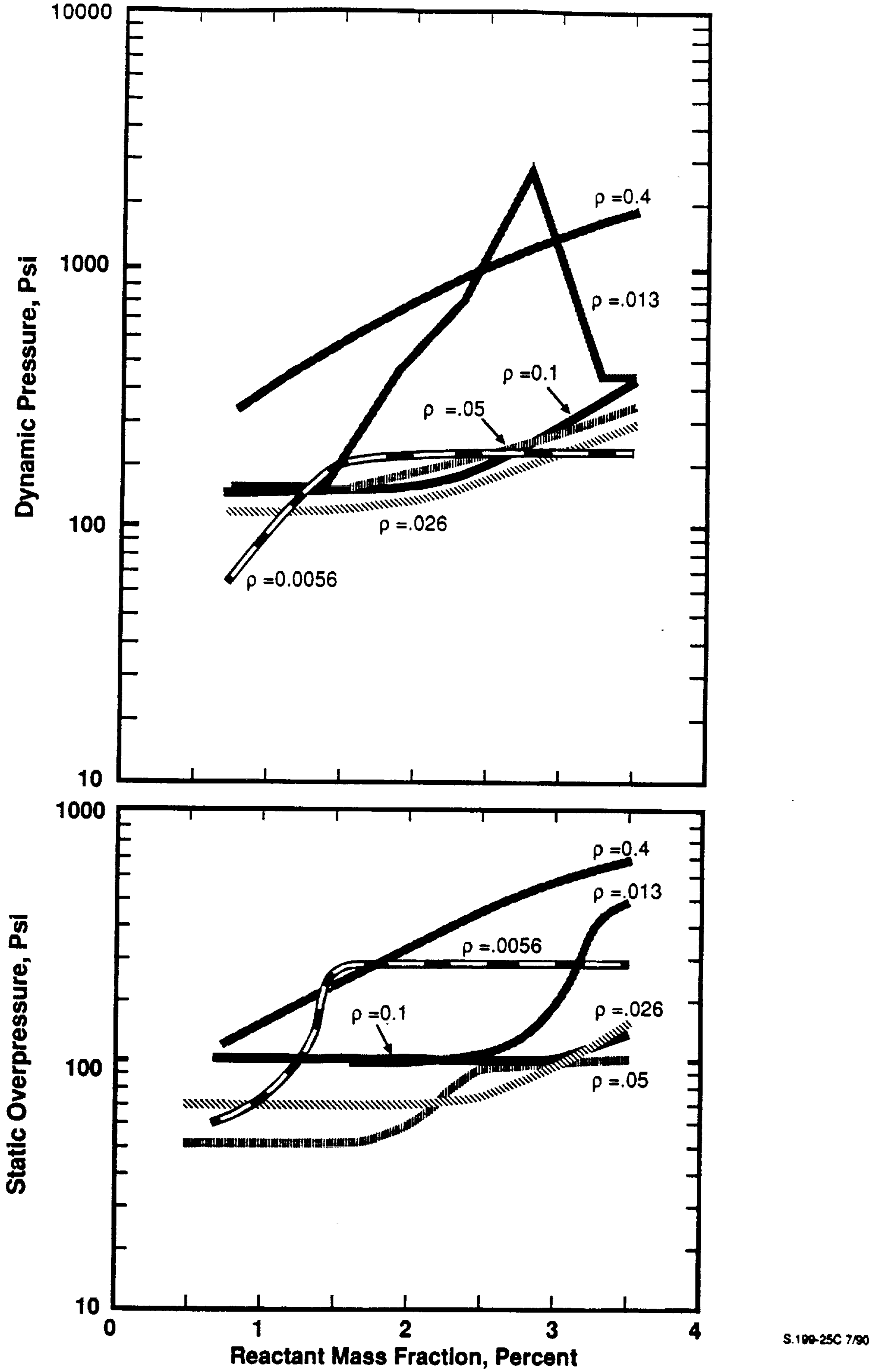

Figure 28. Static and Dynamic Pressure Generated at the CRAF RTG Location For a Number of Assumed Reactant Initial Conditions(1)

(1) Explosion Location and Reactant Geometry Cause Significant Scatter in These Results

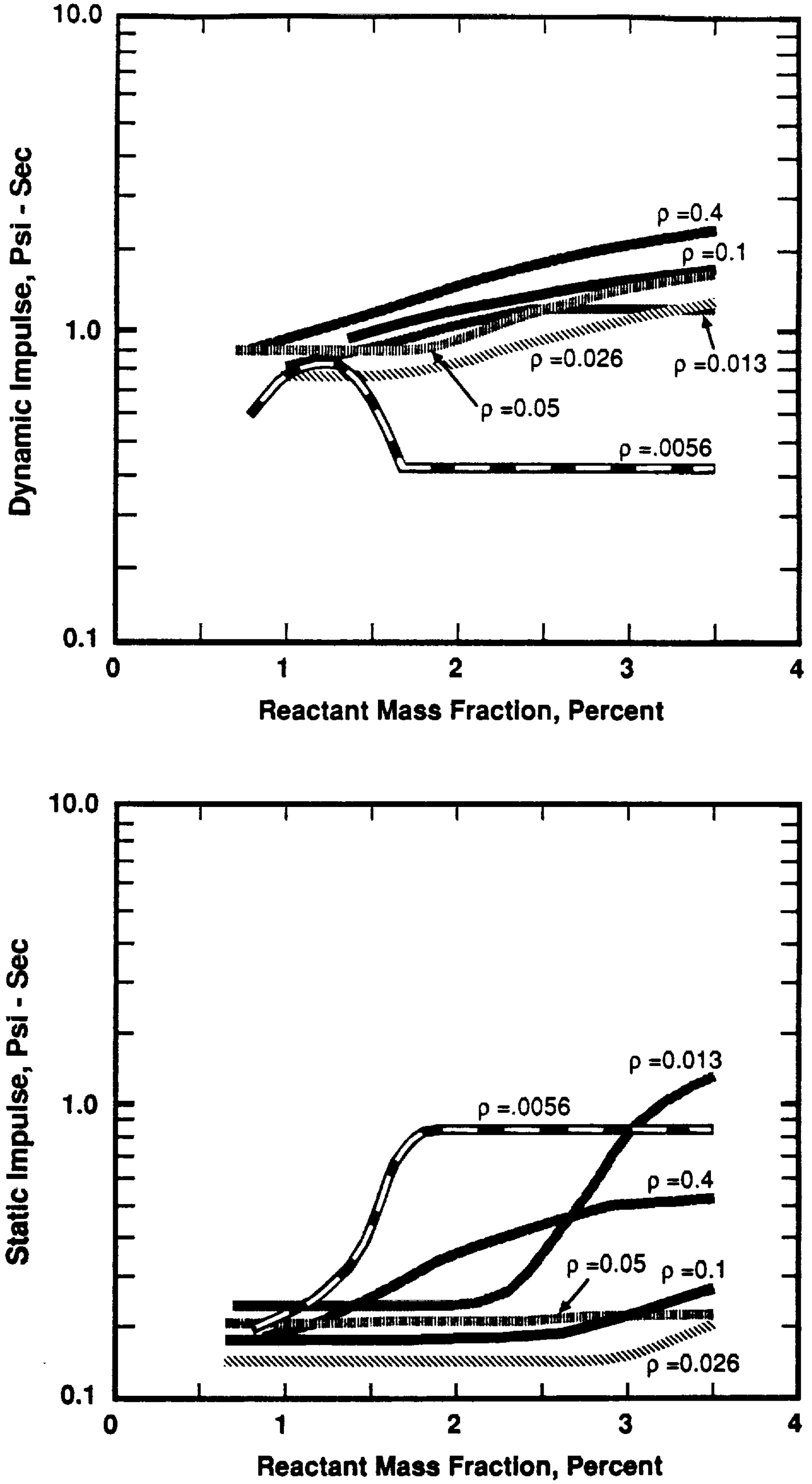

Figure 29. Static and Dynamic Impulse Generated at the CRAF RTG Location For a Number of Assumed Reactant Initial Conditions(1)

(1) Explosion Location and Reactant Geometry Cause Significant Scatter in These Results

Table VII. Probability Distribution Function for Charge Density and Mass Fraction

CUMULATIVE PROBABILITY	CHARGE DENSITY gm/cc	CHARGE MASS FRACTION Percent
0.02	-	0.5
0.08	-	1.0
0.18	-	1.5
0.209	0.00100	-
0.32	-	2.0
0.50	-	2.5
0.667	-	3.0
0.786	-	3.5
0.850	0.00308	-
0.875	-	4.0
0.944	-	4.5
0.985	0.00578	-
0.99982	0.05	-
0.99996	0.20	-
0.99998	0.40	-
1.0000	-	5.0

S-199.14C 12-89C

The results of the hydrocode analysis were digitized and four bivariate arrays were constructed for static overpressure, static impulse, dynamic pressure and dynamic impulse as a function of reactant density and mass fraction of the reactants. The bivariate arrays were then fed into a bivariate interpolation routine. The randomly generated density and mass fractions were used as input to the interpolation routine and values for overpressure, static impulse, dynamic pressure and dynamic impulse were extracted. This process was repeated for each of 10,000 trials and a cumulative probability function was computed for each of the four variables.

The results of the Monte Carlo analysis are presented in Table VIII. Curves of the cumulative probability of the static and dynamic overpressure at the CRAF RTG location are presented in Figure 30. Curves of the cumulative probability of static and dynamic impulse at the same location are shown in Figure 31.

Table VIII. Probability of Various CRAF Location Environments Resulting from the Explosion of Various Amounts of Centaur G′ Cryogens under the Titan IV Shroud.

PROBABILITY	STATIC OVER PRESSURE PSI	DYNAMIC PRESSURE PSI	STATIC IMPLUSE PSI-SEC	DYNAMIC IMPLUSE PSI-SEC
0.05	82.	84.5	0.164	0.372
0.9	164.	184.	0.295	0.766
0.99	400.	1240.	0.653	1.67
0.999	617.	2320.	0.805	2.07
MAX. DRAW(1)	640.	2480.	1.30	2.14

(1) Maximum value drawn in 100,000 attempts.

S-199.23C 8-90C

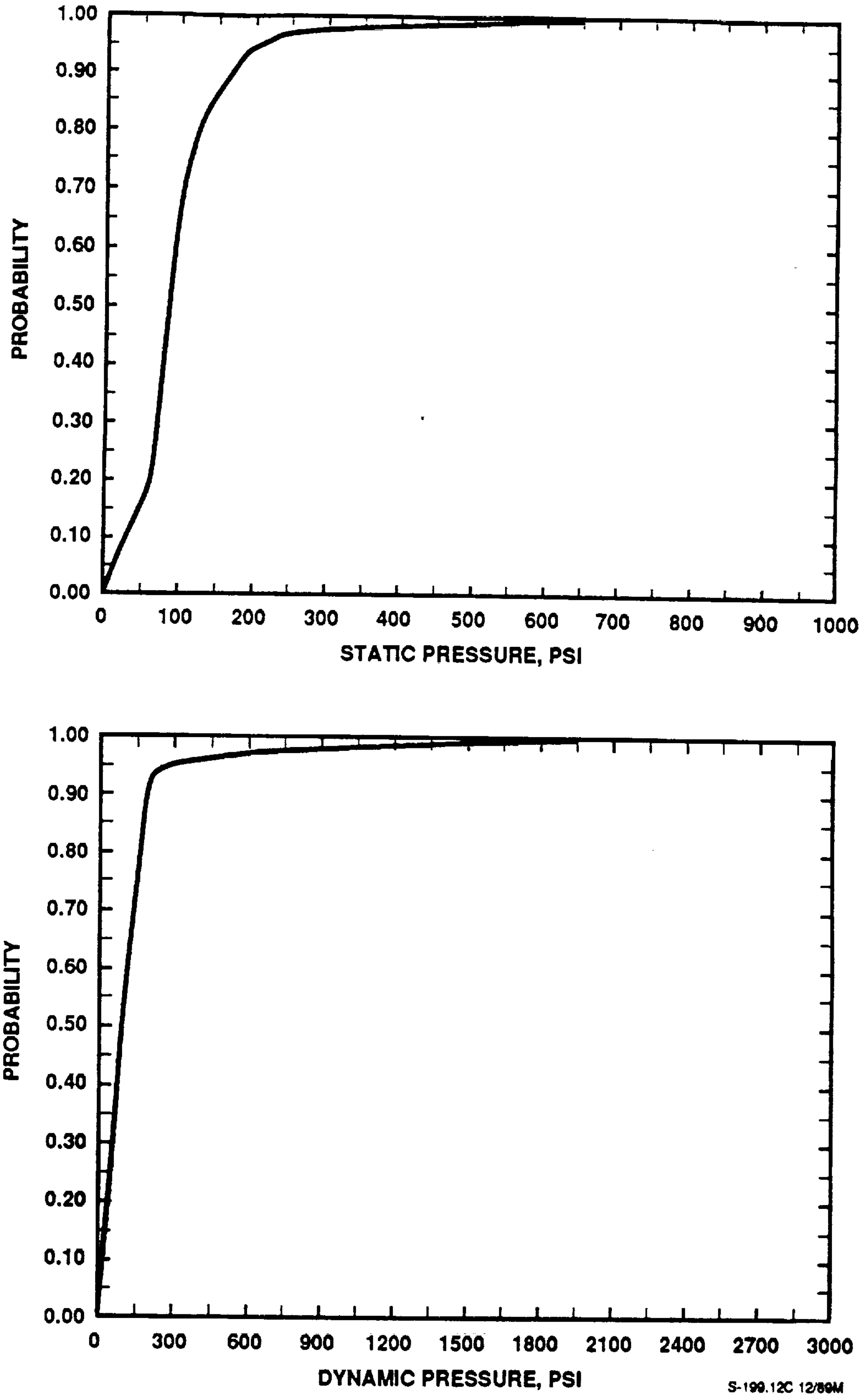

Figure 30. Cumulative Probability of Static and Dynamic Overpressure at the CRAF RTG Location Resulting From a Centaur G' LH_2-LO_2 Explosion Under a Titan IV Shroud.

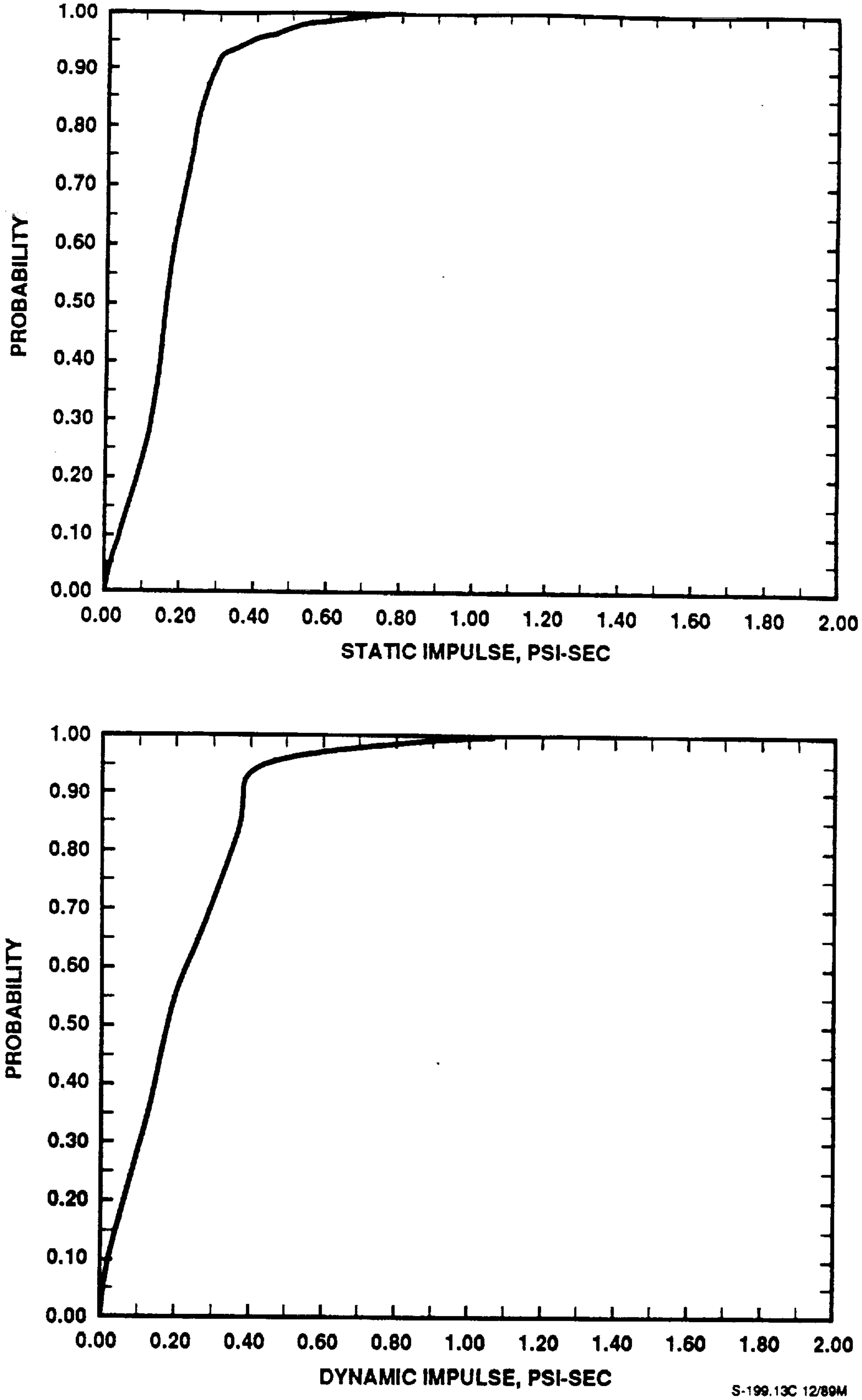

S-199.13C 12/89M

Figure 31. Cumulative Probability of Static and Dynamic Impulse at the CRAF RTG Location Resulting From a Centaur G' LH_2-LO_2 Explosion under a Titan IV Shroud.

REFERENCES

[1] Report AFRPL-TR-68-92, Section 5, Cryogenic Propellant Program.

[2] Tomie, E. J., Personal Communication at presentation in Las Cruces, NM, October 1989.

[3] Lehto, D.L., Personal Communication at Naval Surface Warfare Center in 1986.

[4] Schaefer, G. J., Databook Chairmen. Titan IV Radioisotope Thermoelectric Generator Safety Databook. Volume V, March 1989.

[5] Tomie, E. J., "Propellant Explosive Hazards Study", Vol. 1-3. Aerospace Report No. TOR-0089(4025-04)-1, Rev. A, October, 1989.

[6] Benz, F., Personal Communication. NASA/White Sands Test Facility, Las Cruces, New Mexico, August 1989.

[7] Benz, F. and M. Plaster, Personal Communication. NASA/White Sands Test Facility, Las Cruces, New Mexico, August 1989.

[8] Cull, T.A., T.G. George, and D. Pavone. "General-Purpose Heat Source Development: Safety Verification Test Program", LA-10697-MS. Los Alamos National Laboratory, Los Alamos, New Mexico, September 1986.

[9] Cook, M.A. and L.L. Udy, Detonation Pressure of Liquid Hydrogen/Liquid Oxygen, Intermountain Research and Engineering Co., Salt Lake City, UT. Contract No. NAS8-5058, 1962.

[10] Benz, F., Personal Communication at NASA/White Sands Test Facility in Las Cruces, New Mexico, May 1986.

[11] Farber, E.A., J.H. Smith, E.H. Watts, "Prediction of Explosive Yield and Other Characteristics of Liquid Rocket Propellant Explosions", NAS10-1255. University of Florida, Department of Engineering, Gainsville, Florida, June 1973.

[12] Pesante, R.E and M. Nishibayashi, "Evaluation of Blast Parameters and Fireball Characteristics of Liquid Oxygen/Liquid Hydrogen Propellents", Aerojet-General Report, 0954-01(01FP), April 1967.

[13] Lehto, D.L. "Calculations of Centaur Propellant Explosions in Space Shuttle Cargo Bay", Rev. 2. Prepared for NASA/Johnson Space Flight Center by Naval Surface Weapons Center, Silver Spring, MD, July 23, 1985.